Coordination Chemistry Reviews 432 (2021) 213717

Contents lists available at ScienceDirect

Coordination Chemistry Reviews

journal homepage: www.elsevier.com/locate/ccr

Review

Ag(I)-thiolate coordination polymers: Synthesis, structures and applications as emerging sensory ensembles

Qian Wang *, Su-Li Dong, Dan-Dan Tao, Zhao Li, Yun-Bao Jiang *

Department of Chemistry, College of Chemistry and Chemical Engineering, The MOE Key Laboratory of Spectrochemical Analysis and Instrumentation, and Collaborative Innovation Center of Chemistry for Energy Materials (iChEM), Xiamen University, Xiamen 361005, China

ARTICLE INFO

Article history:
Received 29 August 2020
Received in revised form 10 November 2020
Accepted 11 November 2020
Available online 23 December 2020

Keywords:
Ag(I)
Thiolate
Argentophilicity
Coordination polymers
Sensor

ABSTRACT

As emerging sensory ensembles, Ag(I)-thiolate coordination polymers have been drawing great research interests in the past few years. Ag(I)-thiolate coordination polymers feature unique physical properties such as semiconductivity, luminescence, photothermal and thermochromic effects, which could be leveraged to build physical and chemical sensors, as well as novel multifunctional biomaterials. This review summarizes the synthesis, structures and applications of Ag(I)-thiolate coordination polymers as sensory ensembles towards physical parameters such as temperature and light and chemical analytes including ions, VOCs, amino acids and saccharides. Developments of functional hydrogels for chemosensing and *in situ* drug delivery are also discussed.

Contents

* Corresponding authors.
E-mail addresses: wqchem@xmu.edu.cn (Q. Wang), ybjiang@xmu.edu.cn (Y.-B. Jiang).

https://doi.org/10.1016/j.ccr.2020.213717
0010-8545/

1. Introduction

Silver ion has long been recognized for its bactericidal activity and low toxicity toward mammalian cells [1]. As a consequence, metallic silver and silver compounds have been used as antimicrobial reagents in drinking water, food/water storage recipients, and anti-infectives [1–3]. Ag(I), as a soft acid, has a flexible coordination geometry and rich coordination numbers ranging from 2 to 7 [4], tending to coordinate with soft bases and thus exhibiting a high affinity to inorganic and organic sulfur. Upon coordinating with sulfur, Ag-S bonding allows the formation of many types of ensembles of structural diversity and flexibility [3,5], such as supported self-assembled monolayers on metallic silver (SAMs) [6], thiolate functionalized silver nanoparticles, Ag(I)-thiolate clusters [7–9], and Ag(I)-thiolate coordination polymers [10]. Ag(I)-thiolate coordination polymers consist of Ag(I) containing nodes and various thiolate containing organic linkers through various supramolecular interactions such as metal–ligand interactions, π-π interactions, metal–metal interactions (argentophillic attractions), metal-π interactions, coulombic interactions, and anion bridging [11]. Particularly, the metal–metal interactions (metallophilic interactions) are termed for the phenomena that d^8 or d^{10} metal cations tend to exhibit attractive interactions rather than repulsion when their distance is shorter than the sum of their van der Waals radii, for example shorter than 3.44 Å for silver cations [12–14]. Structurally, the Ag(I)-thiolate coordination polymers can mainly be divided into three groups [15], one dimensional chain coordination polymers, two dimensional lamellar coordination polymers, and three dimensional metal organic frameworks (MOFs) [16,17], the latter are also termed as metal organic chalcogenolates (MOCs). It is worth indicating that Ag(I)-thiolate clusters and nanoparticles, other than just simple silver ions, could serve as building blocks to build coordination polymers. An elegant example is silver chalcogenide clusters based MOFs (SCC-MOFs) that have been developed for sensing VOCs and gas [18]. For the thiolate containing organic linkers, simple ligands including alkyl thiolate, aromatic thiolate, mixed thiolate ligands containing N/P/O atoms such as pyridine/phosphine thiolates [19], even more complicated sulfhydryl amino acids have been utilized to form the Ag(I)-thiolate based coordination polymers.

Ag(I)-thiolate coordination polymers have shown various physical properties [20] such as semiconductivity, luminescence, photothermal and thermochromic effects, which have been applied for chemical sensing, catalysis, separation and functional biomaterials for *in situ* drug delivery [21–27]. Recently, Ag(I)-thiolate coordination polymers have drawn great attention in the development of sensory materials of high selectivity and sensitivity towards various species or external physical stimuli. Ag(I)-thiolate coordination polymers as emerging sensory ensembles feature unique advantages in the following aspects. (i) The intrinsic flexibility and various coordination geometry between Ag(I) and the ligands ensure high sensitivity towards sensing species; (ii) the Ag(I)-thiolate coordination polymers are assembled from building blocks through cooperative weak interactions, that signal amplification and selectivity enhancement are expected; (iii) the structural diversity of 2D and 3D Ag(I)-thiolate coordination polymers offers large surface areas and tunable porosity, beneficial to high efficiency capture and concentration of the analytes; and (iv) particularly, the *in situ* generated chromophores in the Ag(I)-thiolate coordination polymeric backbone, relating to the argentophillic attractions, provide a facile and unique sensing scheme of no spectral background.

Demessence and co-workers summarized d^{10} coinage metal chalcogenolates in terms of the structural dimensionality from 0D to 3D [28]. Yet we have not been able to find reviews describing recent developments of the Ag(I)-thiolate coordination polymers focusing on their structure–property relationship and sensory applications. We therefore consider it is of significance to review the synthesis, structures and applications as sensory ensembles of the Ag(I)-thiolate based coordination polymers, to provide insights in rational designing of those novel sensing platforms and functional materials. This review is thus constructed in four parts. The first part presents the structure, synthesis and characterizations of Ag(I)-thiolate based coordination polymers ($[Ag(SR)]_n$), according to the types of the substituent (R) in the thiolate ligand (RSH) and n is a defined number for the complexes or it is infinite for the coordination polymers; in the second part, applications of Ag(I)-thiolate coordination polymers as physical sensors, for thermochromic and photothermal sensing are summarized; in the third part, applications of Ag(I)-thiolate coordination polymers as chemical sensors are reviewed, for sensing of ions, VOCs, amino acids and saccharides; and finally in part four, Ag(I)-thiolate coordination polymers as multifunctional hydrogels for chemosensing and *in situ* drug delivery are discussed.

2. Synthesis and structures

In Ag(I) coordination polymers, S atom from the thiol ligand mainly acts as μ_2, μ_3 or μ_4 bridge when coordinating with Ag atom [28]. According to the coordination environments, Ag atom adopts diverse geometries, *i.e.* linear, zigzag, triangular, planar square, tetrahedron, cone and even octahedron. XRD, Raman, UV absorption, FTIR, ^{13}C NMR and ^{109}Ag NMR have been employed to study their structures. In this part, Ag(I)-thiolate coordination polymers are classified according to the ligands, in terms of alkyl, aromatic, pyridine/phosphine thiolate ligands, bis(thio)methane ligands, and sulfhydryl amino acids (Scheme 1). The influence of alkyl chain length and branching degree of the substituent (R), temperature, solvents, counteranion will be discussed. More importantly, the stacking modes of the Ag-core and Ag-S unit, lengths of the Ag-Ag/Ag-S bond, and argentophilic interactions in those complexes/-coordination polymers will be discussed, which largely determine the chemical/physical properties of the supramolecular ensembles. It is expected that the general rules summarized in this review would inspire new efforts to rationally design the Ag(I)-thiolate supramolecular architectures of diverse structures and new functions.

2.1. Alkylthiolate ligands

Researches on silver-alkylthiolate complexes/coordination polymers ($[Ag(SR)]_n$) started as early as 1960 s by Åkerström [29]. He determined the molecular weight of silver alkylthiolates in benzene and found that the degree of polymerization (n) relates to the branching degree of the alkyl substituent (R) at α-C atom. When R is a tertiary alkyl group, the complex is octameric (n = 8) with good solubility. With secondary alkyl substituents, the silver thiolate is dodecameric (n = 12). However, when S atom is bound to a primary alkyl chain, the solubility of $[Ag(SR)]_n$ is poor that the degree of polymerization could not be obtained. Early results from Åkerström established a relationship between the polymerization degree n and alkyl chain branching. In the next few years, more crystal structures of $[Ag(SR)]_n$ were obtained that allowed the arrangements of Ag and S atoms and the effect of the substituents on structural dimensionality more clearly analyzed. In the following sections, we will describe alkylthiolate-based silver alkylthiolate coordination polymers in terms of the alkyl chain length, conformation and branching degree of the alkyl substituents, to go deep into their structural characteristics.

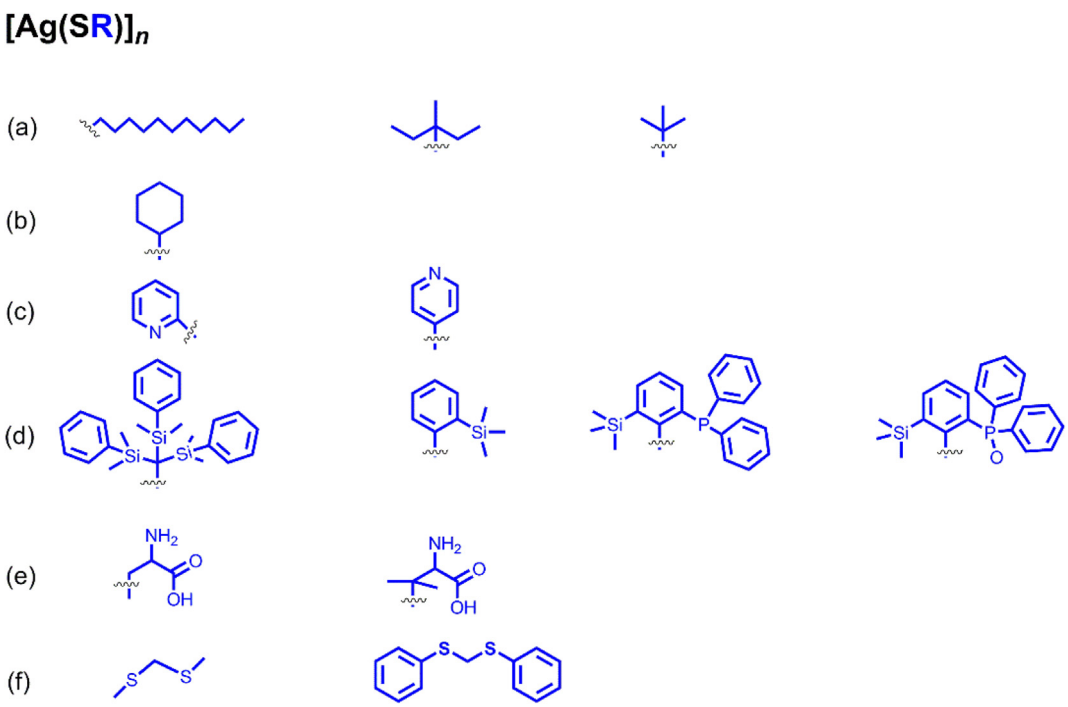

Scheme 1. Chemical structures of substituents R in $[Ag(SR)]_n$ presented in the synthesis and structure part. (a) alkyl substituents, (b) cyclohexane substituent, (c) pyridyl substituents, (d) aromatic substituents, (e) amino acid substituents and (f) bis(thio)methane ligands.

2.1.1. Primary alkylthiolate ligands

Conformation of primary alkyl chain in the thiolate ligand has an important effect on the structure of $[Ag(SR)]_n$. Natan and co-workers [30] prepared a layered solid $AgS(CH_2)_3CH_3$ (**1**) with three different forms, the fully extended *trans* (T) form, *gauche* (G) isomer and T/G mixture, depending on the conformation of the alkyl chain (C1-C2 bond) (Fig. 1 (a, b)). All of those compounds consist of alternative arrangement of Ag(I) and S atoms, with alkyl chains extending on both sides of the Ag-S-Ag-S chains, further stacking into layered structures. For all-*trans* **1**, Ag atom is distorted and coordinated by two or three S atoms with an interlayer spacing of 15.56 Å. In the *gauche* form, strictly planar geometry is adopted for each Ag atom, linked by three S atoms with a 16.88 Å interlayer spacing. Both of the two interlayer spacings are present in the T/G mixture. Compared to all-*trans* compound, the *gauche* form exhibits an attractive character that there is 50% per layer vacancy, taking up more interlayer space. The *trans*-conform is unstable and is able to translate to the *gauche* form, evidenced by the temperature-dependent color change from white to bright yellow, arising from the low-energy ligand-to-metal charge transfer (LMCT) bands.

Zhou's group [31] studied the structures of $AgS(CH_2)_nCH_3$ (**2**) with a longer alkyl chain of n ranging from 7 to 18 (Fig. 1 (c, d)). The layered materials centered on Ag(I) and S atoms with alkyl chains extending up and down, similar to that seen in the Ag(I)-butanethiolate complexes reported by Natan *et al.* [30]. The interlayer spacing increases with increasing length of the alkyl chain and a linear relationship is established, with a slope k = 2.48 ± 0.02 Å (per pair of CH_2 group), slightly lower than that expected (2.54 Å) for all-*trans* alkyl chain. This indicates that the alkyl chains are tilted by 12 ± 3° relative to the surface normal and is confirmed by calculated of IR spectrum. Ag and S atoms in **2** are arranged in a distorted hexagonal lattice, slightly different from that in the silver-butanethiolate complexes **1**. This is mainly because of the thermostability and high order of alkyl chains, which afford all-*trans* and close-packed form. In another way, Ag atom coordinates with two S atoms in **2** in the S-Ag-S diagonal mode, other than the previously reported trigonal geometry by Natan *et al.* [30].

Swanson and co-workers [32] reported Ag(I)-alkanethiolates $AgS(CH_2)_nCH_3$ complexes (**3**) of n = 5, 6, 9, 11, 15 and 17. Structural studies show that Ag and S atoms in the thiol ligands are coordinated in a trigonal geometry, resulting in a quasi-hexagonal inorganic core of about 1 Å thickness (Fig. 1 (e, f)). The alkyl chains in all-*trans* conformation are self-assembled into a sandwich-shaped arrangement between Ag-S backbones, similar to that reported by Zhou *et al.* [30]. The alkyl chains in each assembly are vertical to the hexagonal Ag-S lattice. Regular one-dimensional channels form between adjacent layers. Together with previous models proposed by Natan *et al.* [29], a two-step, hierarchical self-assembly mechanism for $[Ag(SR)]_n$ was proposed. Firstly, Ag atoms are linked by alkanethiolate ligands into a symmetrically folded quasi-hexagon two-dimensional lattice, with alkyl chain extending on each side. Then, the two-dimensional building units form a sandwich bimolecular chain assembly in the third dimension *via* a secondary complementary stacking of the alkyl chains.

2.1.2. Secondary and tertiary alkylthiolate ligands

Dancer's group [33] described in detailed on $[Ag(SR)]_n$ coordination polymers containing a tertiary alkyl thiol ligand, 3-methylpentane-3-thiol. One-dimensional chain structure consisting of alternative Ag(I) and S atoms in the form of planar zigzag -Ag-S-Ag-S- form is seen in **4** (Fig. 2 (a, b)). Two unconnected $(-Ag-SR-)_n$ strands are surrounded and separated by the alkyl substituents, forming one polymer chain in two planes: the Ag_3 fragment of the chain in one plane that twists out of the plane by coordinating with Ag_5 or Ag_6 atoms in the other plane. The shortest distance of the Ag(I)-Ag(I) contacts between the two strands is 2.889 Å, suggesting the occurrence of Ag(I)···Ag(I) interactions. Unlike that of the primary alkyl substituted $[Ag(SR)]_n$, Ag(I) atoms adopt a linear geometry with the angles of S-Ag-S varying in the range of 169° to 178°, meaning that the Ag(I) bonding is fulfilled by two S atoms without secondary Ag-S bonding.

For silver thiolates with poor solubility and crystallinity, one way to get the crystals suitable for structural characterization is

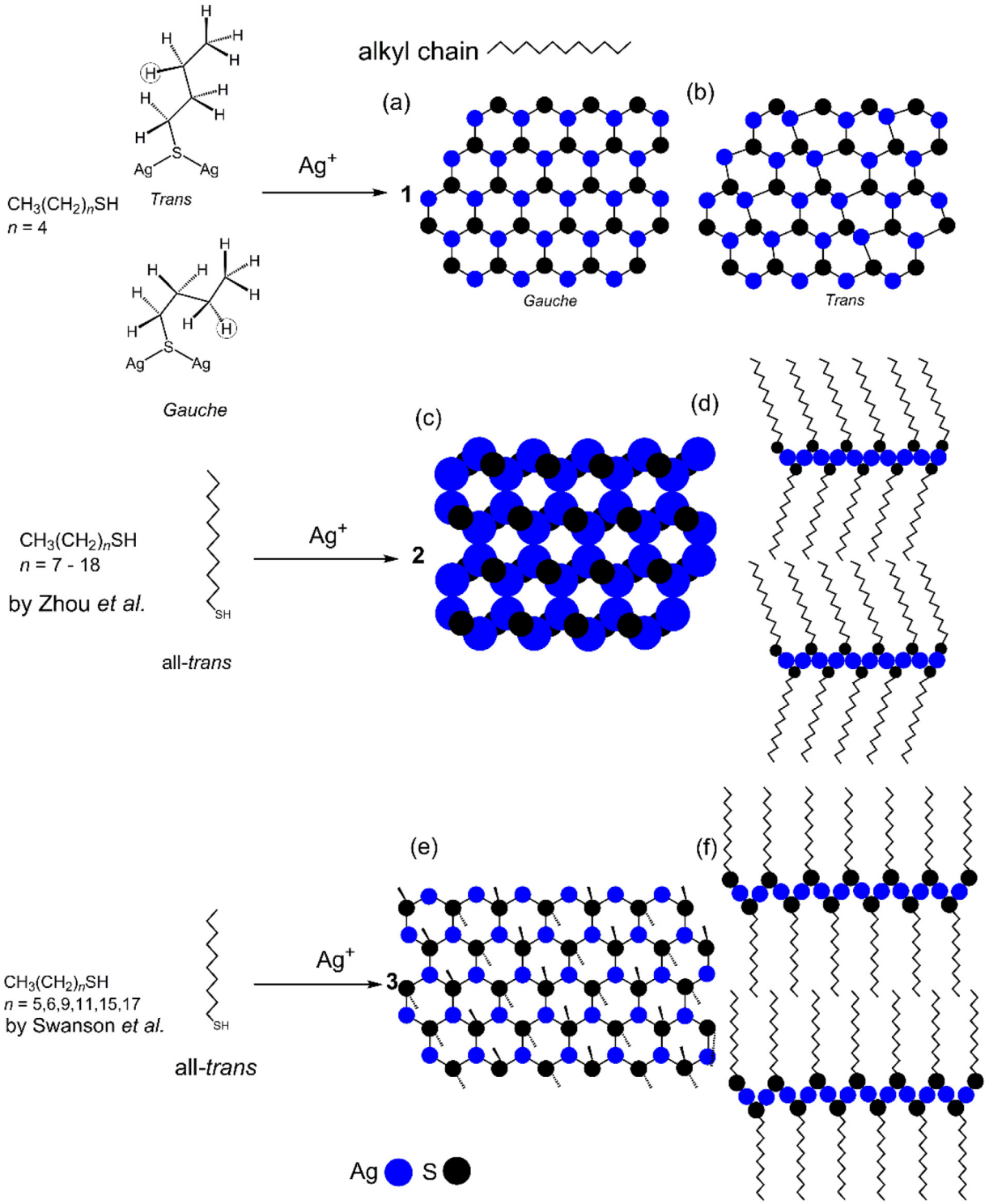

Fig. 1. Proposed configuration and arrangements of S and Ag atoms of **1** with short alkyl chains in (a) *gauche* and (b) all-*trans* conformations depending on the orientation of alkyl chain. Proposed arrangement of S and Ag atoms and layered structure of **2** reported by Zhou *et al.* (c, d) and **3** by Swanson *et al.* (e, f) with long alkyl chains. The ligands are omitted for clarity. Reprinted with permission from Refs. [30], [31] and [32].

to increase the branching degree of the substituent R in the thiolate SR [29], and the other way is to introduce bulky auxiliary ligands. Benefiting from this strategy, crystal structures of $(AgSC_6H_{11})_{12}$ [34] and $(AgSCMeEt_2)_8$ [33] containing respectively the secondary and tertiary alkyl substituents have been obtained. Tertiary phosphine was introduced as an ideal structure-determining auxiliary ligand. Dance *et al.* [35] prepared two silver thiolates $(AgSCMeEt_2)_8(Ph_3P)_2$ (**5**) and $(AgS\text{-}Bu^t)_{14}(Ph_3P)_4$ (**6**) from reaction of triphenylphosphine and silver tertiary alkanethiolates (Fig. 2 (c,d)). **5** contains two different cyclic silver rings: $(\mu\text{-}SCMeEt)_4(Ag^{dig})_4$ from four Ag^{dig} (dig refers to diagonal) atoms (Ag_5, Ag_6, Ag_7, Ag_8) and $(\mu\text{-}SCMeEt_2)_4\text{-}(Ag^{dig})_2(Ph_3PAg^{trig})_2$ that consist of two Ag^{dig} atoms (Ag_3, Ag_4) and two Ag^{trig} (trig refers to trigonal) atoms (Ag_1, Ag_2). The two rings are further linked with

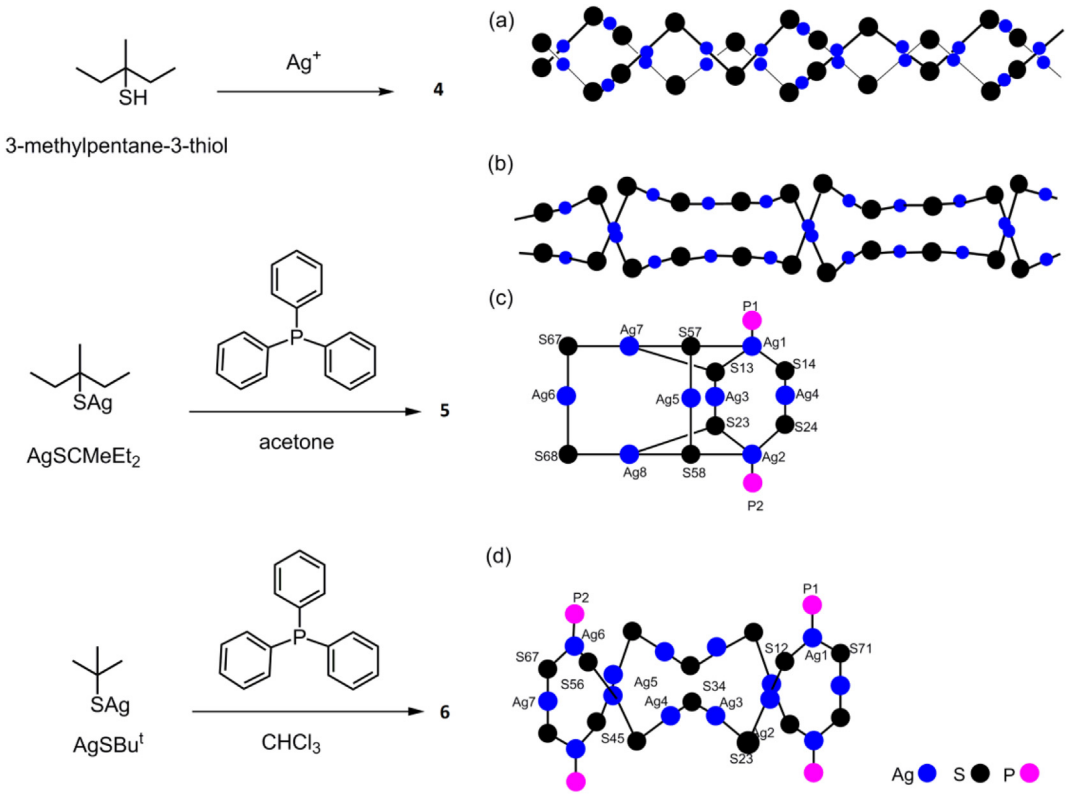

Fig. 2. Proposed Ag and S atom arrangement of two uncontacted zigzag strands of **4** from two different views (a, b), and proposed Ag and S atoms arrangements of **5** (c), **6** (d). The ligands are omitted for clarity. Reprinted with permission from Refs. [33] and [35].

each other by four long secondary Ag-S bonds (Ag_{17}-S_{13}, Ag_8-S_{23}, Ag_1-S_{57} and Ag_2-S_{58}). In this structure, there are 12 primary Ag^{dig}-S bonds with an average length of 2.39 Å, which is almost 0.5 Å shorter than the secondary Ag-S bonds at Ag_7 and Ag_8. For the trigonal silver atoms Ag_1 and Ag_2, the primary Ag^{trig}-S bond length ranges from 2.50 to 2.66 Å, which is ca. 0.4 Å shorter than the secondary connections of 2.90 and 2.97 Å. **6** has a larger 28-membered ring structure that consists of alternative Ag(I) and S atoms, of which Ag^{trig} atoms are coordinated by phosphine ligands. Four segments were identified in the structure of **6**, (a) eight zigzag linear segments in the opposite faces; (b) four linear crossover segments; (c) four trigonal bending segments, and (d) two linear end segments.

2.1.3. Cyclohexanethiol ligand

Hesse *et al.* [34] obtained crystal structure of Ag(I) cyclohexanethiolate $[Ag(SC_6H_{11})]_n$ (**7**) (Fig. 3). Chains consisting of Ag(I) and S atoms extend in *c*-direction and are separate from each other by the surrounding cyclohexyl groups. Both two-coordinated and three-coordinated Ag(I) atoms are formed in the structure of **7**. Degree of association is n = 25, which is larger than those of most of the other complexes of secondary alkyl thiolates of Ag(I) (n = 12), determined by Åkerström [29]. The Ag(I) atoms exist in two parallel strands, which are related by a centre of symmetry and crosslinked through four Ag atoms. The distances of the Ag(I)-Ag(I) contacts range from 2.91 to 3.11 Å in the chains and 3.03 to 3.29 Å in the crosslinks, in both cases Ag(I)···Ag(I) interactions occur. For the Ag(I) atoms in this complex, eight of them adopts almost planar coordination with three other atoms, while four of them have two-fold coordination with two S atoms in a nearly linear manner, similar to those reported in previous investigations [36].

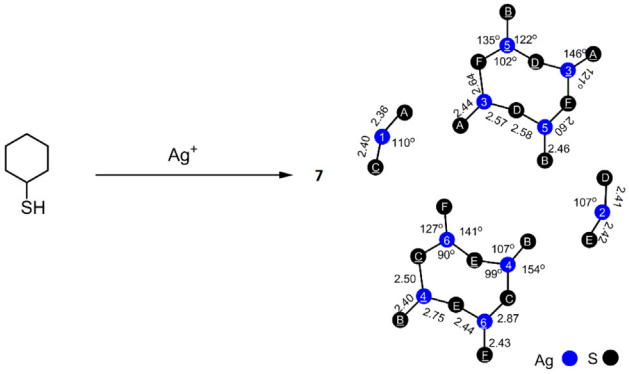

Fig. 3. Proposed Ag and S atom arrangements of **7**. The ligands are omitted for clarity. Reprinted with permission from Ref. [34].

2.2. Pyridyl thiolate ligands

Typically, protonated and non-protonated N atoms in pyridine-2-thiol both exist in the forms of pyridine-2-thiolate and 1H-pyridine-thione. Pyridine-2-thiolate could take three coordination modes (Fig. 4), while 1H-pyridine-thione acts only as a μ_2 bridge through S atom to coordinate with two Ag(I) atoms.

Reaction of $AgBF_4$ with pyridine-2-thiol in DMF/H_2O at 0 °C produces colorless thin sheet-liked crystal of $[Ag(C_5H_4NS)]_n$ (**8**), while yellow crystal of $[Ag(C_5H_4NS)(C_5H_5NS)BF_4]_n$ (**9**) when the reaction is performed in CH_3CN at room temperature [37]. **8** is a two-dimensional lamella structure that consists of Ag(I) arranged in graphite-like array thus showing excellent semiconductivity, similar to that of $Ag_6(BTC)_2(APYZ)_6{\cdot}9H_2O$ by Sun *et al.* [38] and of $[Ag_2(H_2trzS)_2Cl_2]_n$ by An *et al.* [39]. PyS^- ligand serves as a μ_3 bridge to link three Ag atoms through two S atoms and one N atom (Fig. 4

(a)) in the structure of **8**, in which Ag(I)···Ag(I) interactions exist accounting for its conductivities. Unlike that in **8**, the array in the two-dimensional network of **9** is relatively irregular, with Ag-Ag bond length varying from 2.995 to 3.810 Å, therefore exhibiting no conductivity property. Three coordination environments are discovered in **9**: $AgNS_2$ with distorted planar trigonal geometry and $AgNS_3$ and AgS_4 with distorted tetrahedral geometry. These results show that the reaction conditions such as temperature and solvent are important for the formed structures of the Ag(I)-thiolate coordination polymers.

Two coordination polymers with distinct structures of $[Ag_4(C_5H_4NS)_2(NO_3)_2]_n$ (**10**) and $[Ag_3(C_5H_4NS)_2]_n{\cdot}nClO_4$ (**11**) were obtained from the *in situ* reaction of C_5H_4NS ligand with silver ion of counteranions NO_3^- and ClO_4^-, respectively [40] (Fig. 4 (b) and (c)). One N atom of pyridine-2-thiol coordinates with one Ag(I), while S atom acts as a μ_3 or μ_4 bridge with silver. Both **10** and **11** have a binuclear Ag(I) cluster as the basic building block, strongly supported by the Ag(I)···Ag(I) interactions (distance of Ag(I)-Ag(I), 2.899 Å), a fact not discovered in the connections of the neighboring binuclear clusters. The counteranions of NO_3^- and ClO_4^- play different roles in the formation of the coordination polymers **10** and **11**. In **10**, NO_3^- coordinates with metal ion generating two-dimensional networks, while ClO_4^- in **11** does not coordinate with any metals, but only functions as a counteranion in the 2D architecture. This report highlights the role of counteranion of Ag(I) on the structure of the formed Ag(I)-thiolate coordination polymers.

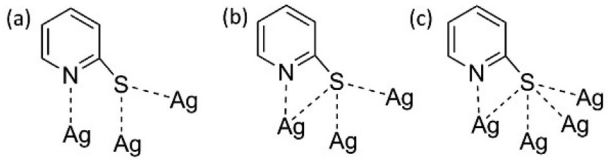

Fig. 4. Coordination model of pyridine-2-thiolates.

Jain and co-workers [41] obtained silver thiolates $[Ag(S\text{-}4\text{-}pyH_{0.5})_2(PPh_3)_2]$ (**12**) and $[Ag_2(\mu\text{-}S\text{-}4\text{-}py)_2(PPh_3)_4]$ (**13**), by reacting $[Ag_2(\mu\text{-}Cl)_2(PPh_3)_4]$ complex with 4-pyridine-SH ligand in the presence of Et_3N and NaOH, respectively (Fig. 5). **12** is a hydrogen bonded chain-like structure, in which Ag(I) atom adopts a distorted tetrahedral configuration that coordinates with two PPh_3 molecules and two S atoms of the 4-pyridine-SH ligands. In this case, one N atom of pyridyl group is protonated with 0.5 proton to maintain a charge balance. Hydrogen bonding is indicated from the short distance of 2.656 Å between two neighboring protonated N atoms of pyridyl group, which promotes the formation of an infinite chain of coordination polymer **12**. On the contrary, **13** is a binuclear structure consisting of a distorted tetrahedral P_2S_2 core and a distorted rhombohedral Ag_2S_2 core, with N atoms of pyridyl group not included in the metal coordination. The distances of Ag(I)-Ag(I) (3.981 and 4.071 Å) are longer than the sum of van der Waals radius in this complex, indicative of no argentophilic interactions. When **13** is heated in methanol, a new two-dimensional coordination polymer $[Ag_2(\mu\text{-}S\text{-}4\text{-}py)_2(PPh_3)_2]_n$ (**14**) forms, which consists of two PPh_3, two S-4-py ligands, and two Ag(I) atoms. Each S atom coordinates with two Ag(I) atoms to form a rhombohedral cycle. Different from that in **12** and **13**, N atom of 4-pyridine-SH in **14** is coordinated with Ag(I) atoms, forming two-dimensional networks. Moreover Ag(I)···Ag(I) interactions in Ag_2S_2 core (Ag(I)-Ag(I) bonds, 2.966 and 3.419 Å) are shown in **14**.

2.3. Aromatic thiolate ligands

The steric effect of the substituent at α-carbon of the thiolate has an important impact on its coordination with Ag(I). As the steric hindrance decreases, the structure of its Ag(I) coordination polymer may varies from simple oligomer to polymer. For example, $[AgSC(SiPhMe_2)_3]_3$ (**15**) with a bulky substituent -C$(SiPhMe_2)_3$ is reported to be in trinuclear structure consisting of Ag_3S_3 core with a 6-membered ring. For complex with a less bulky

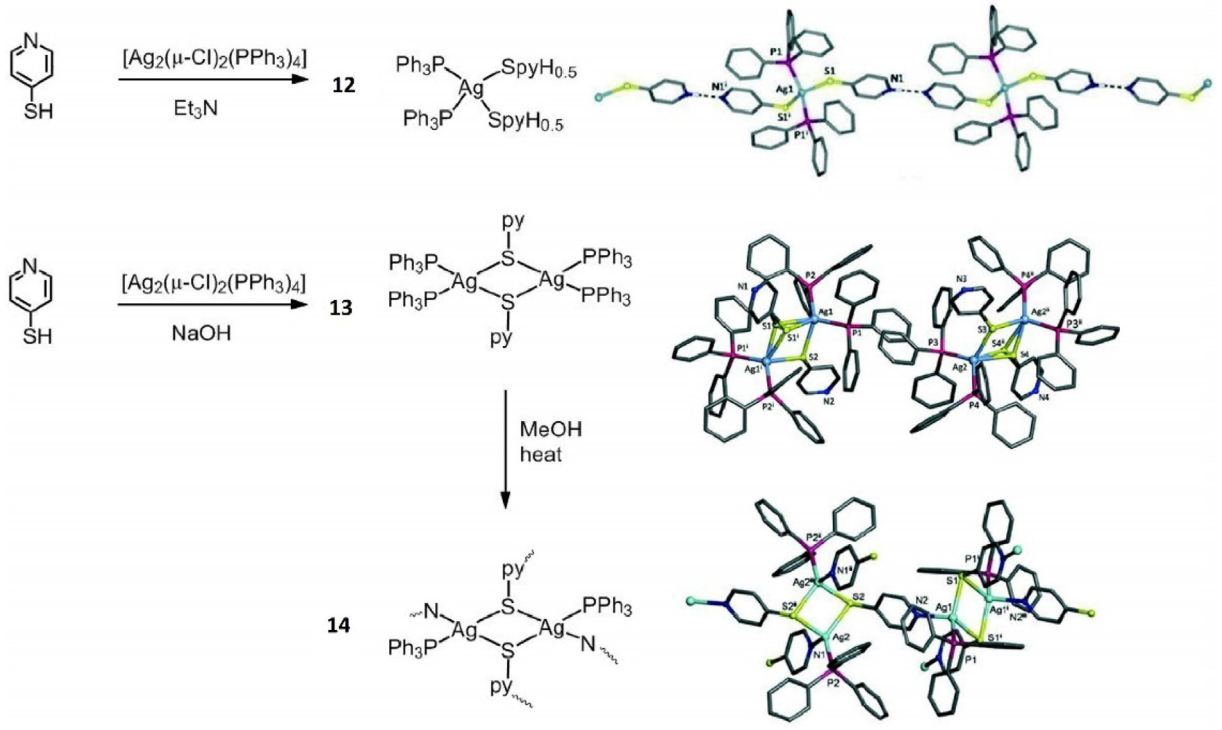

Fig. 5. Proposed structure of **12** supported by hydrogen bond between protonated pyridyl groups, structure of **13**, and part of the network of **14**. Reprinted with permission from Ref. [41].

thiolate ligand of $[AgSC(SiMe_2)_3]_4$ (**16**) a 8-membered cyclic tetranuclear structure is produced. By decreasing the substituent steric hindrance to $HSCH(SiMe_3)_2$, a dicyclic structure of $[\{AgSCH(SiMe_3)_2\}_4]_2$ (**17**) forms, consisting of two tetranuclear $\{AgSCH(SiMe_3)_2\}_4$ rings that are connected by secondary Ag-S bonds (Fig. 6) [42]. It is made clear that, by tuning steric hindrance of the substituent, the degree of polymerization in the metal coordination complex/polymer can be controlled. In other coinage metal such as copper, similar steric effect has also been reported to directly correlate to the degree of polymerization in the coordination polymers, that the thiolate ligand of increasing size leads to lower degree of polymerization [43].

Block and co-workers [44] obtained octamer structure of $[\{Ag(SC_6H_4\text{-}o\text{-}SiMe_3)\}_4]_2$ (**18**) by reacting $HSC_6H_4\text{-}o\text{-}SiMe_3$ with Ag(I). Both similarities and differences are discovered in the structures of **18** with respect to **17**. In **17**, a nonplanar "T" coordination geometry is discovered in the Ag_4S_4 core, with dihedral angle of 78.0° between S(1)Ag(1)S(4)Ag(4)S(3) and S(3)Ag(3)S(2)Ag(2)S(1) planes, compared to 139.6° in **18**. For the orientation of the thiolate substituents, all four substituents are located on the same side of the Ag_4S_4 ring to give an AAAA configuration in **17**. While in **18** three substituents direct to one side while the fourth to the opposite side to minimize the interactions with next Ag_4S_4 ring, assuming an AAAB configuration (Fig. 6). The orientation of the thiolate substituent is shown to define the steric hindrance of $-CH(SiMe_3)$ and $\text{-}C_6H_4\text{-}o\text{-}SiMe_3$.

Besides using bulky groups nest to sulfur atom in the ligand to modify the degree of aggregation of the $[Ag(SR)]_n$ coordination polymers, additional donor atoms such as P, O or N atoms in the thiolate ligands and/or auxiliary or coligand are also applied to tune the structure and degree of aggregation by blocking some of the coordination sites. Ph_2P-based complex $[Ag_4\{2\text{-}(Ph_2P)\text{-}6\text{-}(Me_3Si)C_6H_3S\}_4]$ (**19**) [45] is reported to be a highly distorted tetranuclear complex showing an arrangement of alternative Ag and S atoms. Each Ag atom of the $[AgS_2P]$ core is in distorted triangle environment coordinated by one P atom and two S atoms, laying out of the plane of the phenyl ring. The distance of Ag(I)-Ag(I) with in the range of 2.93–3.53 Å, indicates the occurrence of possibly weak argentophilic interactions. Asymmetric sulfur bridges in **19** are found from the difference in the Ag-S bond length. $[Ag_4\{2\text{-}(Ph_2PO)\text{-}6\text{-}(Me_3Si)C_6H_3S\}_4]$ (**20**) [45] consisting of $\text{-}Ph_2PO$ group, is a distorted parallelogram tetranuclear complex containing four silvers, which are symmetrically located around the inversion center and linked to each other by ligands. The coordination environments of Ag atoms in **20** are: four-fold coordinated Ag atom in $[AgO_2S_2]$ and two-fold coordinated Ag in $[AgS_2]$. Four S atoms are coplanar, with two S atoms above the plane that consist of four Ag atoms and the rest two S atoms below the Ag plane (Fig. 7). The dihedral angle of the S atom-based planes and the Ag atoms-based plane is 167.46°. For complex **20**, the steric influence of the phosphorus groups on the structure is minimized because of the longer Ag-O distances. More significantly, the introduction of the O atom expands the chelate ring {Ag-O-P-C–C-S-}.

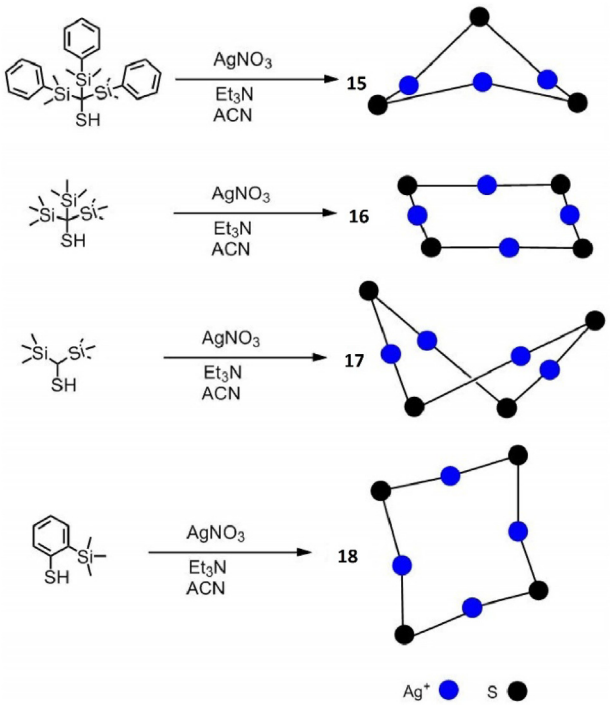

Fig. 6. Proposed Ag and S atom arrangement of Ag_3S_3 core of **15**, cyclic tetranuclear of **16**, tetranuclear ring of **17** and Ag_4S_4 ring of **18**.The ligands are omitted for clarity. Reprinted with permission from Refs. [42] and [43].

2.4. R-S-CH_2-S-R ligands

Brisse and co-workers [46] reported two one-dimensional coordination polymers **21** and **22** using bis(methylthio)methane ligand and $Ag(CF_3CO_2)$ and $Ag(CF_3CF_2CO_2)$, respectively (Fig. 8). Both of the two coordination polymers contain $Ag_{12}S_6$ clusters, in which 12 Ag(I) atoms are placed in the corners of a distorted cuboctahedron. Six S atoms of $\mu_4\text{-}SCH_3$ are located 0.8 Å above the center of the polyhedron plane. The contact distances of Ag(I)-Ag(I) in **21** (2.9250(5) – 3.3615(6) Å) and **22** (2.961(1) – 3.380(1) Å) are shorter than the sum of van der Waa radii 3.44 Å [47], indicating the operation of weak argentophilic interactions. S atoms in **21** adopt two distinct coordination modes, in the bis(methylthio) methane ligand linked by one Ag atom, while one sulfur of $\text{-}SCH_3$ shared by four silver ions. The $Ag_{12}S_6$ clusters in **22** contact each other through the ligand that binds with Ag(1) and Ag(5) atoms of the adjacent clusters, generating thereby a 1D coordination polymers that further stack into a hexagonal array. In the structure of **22**, two H_2O molecules coordinate with Ag(I) atoms, making the cluster slightly different from **21**. The water molecule connects to O atoms of two $CF_3CF_2CO_2^-$ anions, one within the $Ag_{12}S_6$ cluster and the other in adjacent chains by hydrogen bonding, forming a two-dimensional network.

A series of Ag(I) coordination polymers were obtained from bis (phenylthio)methane ligand and Ag(I) of various counteranion of

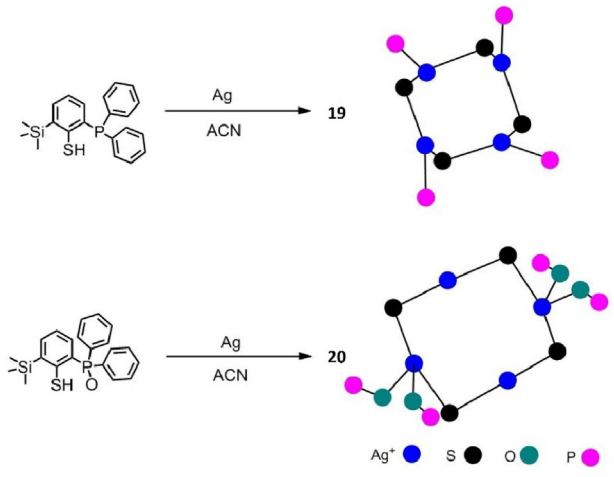

Fig. 7. Proposed Ag and S atom arrangement in **19** and **20**. The ligands are omitted for clarity. Reprinted with permission from Ref. [44].

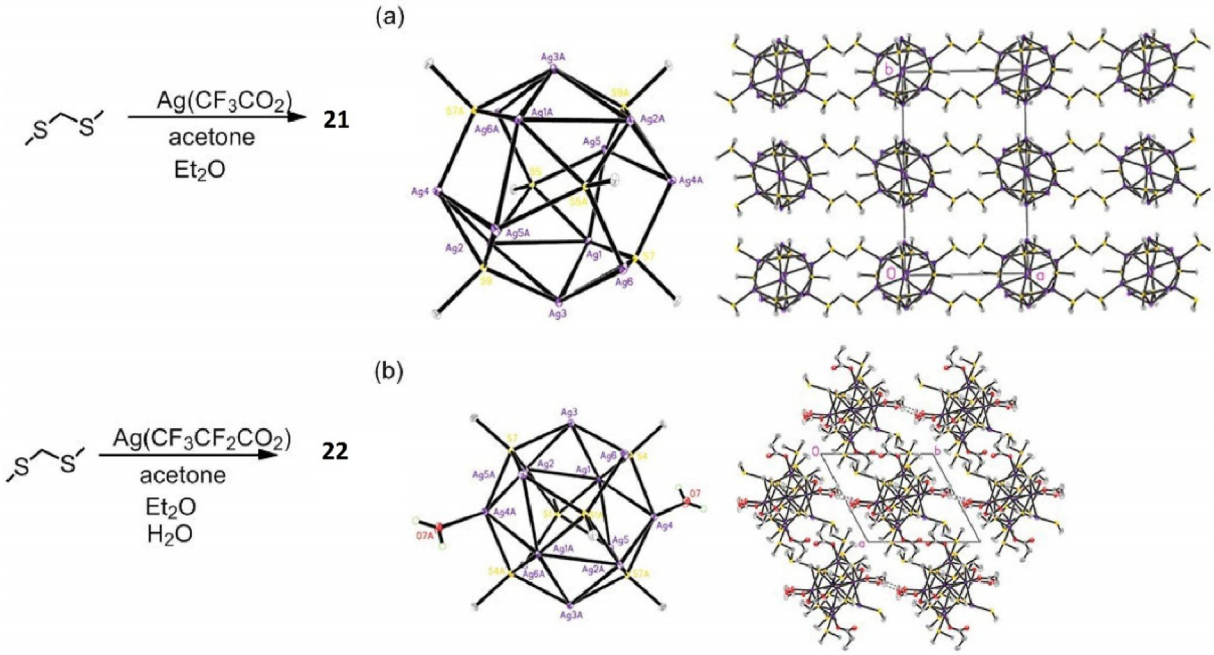

Fig. 8. Structure and Ag and S atom arrangement of **21** (a) and **22** (b). Reprinted with permission from Ref. [45].

ClO_4^- (**23**), BF_4^- (**24**), CF_3COO^- (**25**), $CF_3SO_3^-$ (**26**, **27**), $CF_3CF_2CF_2COO^-$ (**28**), and a diacid, $^-OOCCF_2CF_2COO^-$ (**29**) (Fig. 9), also by Brisse and co-workers [48]. All compounds of **23**–**29** have an one-dimensional structure consisting of alternatively arranged Ag(I) and S atoms in the form of -Ag-S-Ag-S-, which further assembles into two-dimensional-layer structures in different stacking modes *via* van der Waals interactions. In coordination polymers **23**–**26**, Ag coordinated with S atoms are also coordinating with counteranions through single O or F atom, which adopt two different conformations, *gauche-trans-gauche* for **23**, **24** and **26** and *guache-guache-guache* for **25**. **26** can transform into **27** when solvent is changed from diethyl ether to petroleum ether. **27** is a 16-membered macrocyclic structure formed through the connection between small cyclic dimeric unit $(AgCF_3SO_3)_2$. Complex **28** is a double-stranded ladder-like structure. Ag(I)···Ag(I) interactions, as well as C(H)···F or C(H_2)···F (2.998–3.203 A) interactions, are found **29**, as also indicated by the FTIR band around 521 cm^{-1}. For **23**–**26**, different stacking mode of neighboring phenyl groups of the ligands arise from the counteranions, leading to different dihedral angles, 77.4° for **23** and 87.1° for **24** with tetrahedral anions ClO_4^- and BF_4^-, while 59.7(3)° for **26** with non-planar bulk anion $CF_3SO_3^-$. Compound **25**, with near-plane anion CF_3COO^-, has a dihedral angle of 0°. The importance of steric hindrance of the counteranions in defining the stacking modes of the phenyl substitute in ligand and the interactions between the constitutional structural units are nicely shown.

2.5. Sulfhydryl amino acids

Jalilehvand and co-workers [49] reported structures of Ag(I) with sulfhydryl amino acids, cysteine, penicillamine and glutathione (Fig. 10). Crystal structure of $(NH_4)Ag_2$(HCys)Ag(Cys). H_2O (**30**) reveals that it consists of Ag(I)-thiolate layers parallel to *ab* plane. The neighboring layers link each other through hydrogen bonding between O5 atoms of water molecules and N3 atoms of ammonium ions. According to the coordination environments, Ag(I) atoms of each layer are classified into two types: one in the form of *pseudo* tetrahedral AgS_3N and the other in trigonal AgS_3. Ag(HPen)·H_2O (**31**) is a double-helical chain with the two nearly linear -S-Ag-S-Ag- strands intertwining, driven by weak interactions with nearby carboxylate oxygen atoms. Both the structures of **30** and **31** are supported by the Ag(I)···Ag(I) interactions. When structures were obtained in alkaline aqueous solutions and Ag(I)-glutathione at ligand/Ag(I) molar ratio of 2.0 to 10.0 (at Ag(I) concentration of 0.01 M), Ag atom is diagonally coordinated by two S atoms with an average Ag-S bond length of 2.36 ± 0.02 Å. For Ag(I)-cysteine at ligand/Ag(I) molar ratio of 2.0–10.1 (at Ag(I) concentration of 0.1 M), Ag(I) atom is three-fold coordinated by S atoms with an average Ag-S bond length of 2.45 ± 0.02 Å. Unlike that in the two above mentioned complexes, Ag-S bond length in Ag(I)-penicillamine complex increases from 2.40 to 2.44 ± 0.02 Å with increasing ligand/Ag(I) molar ratio from 2.0 to 10.0. This reflects a change in the coordination environment of Ag atom, from AgS_3 to AgS_2 form, which is evidenced by ^{109}Ag NMR resonance at 922 ppm and an average Ag-S length of 2.40 ± 0.02 Å in the AgS_2 unit.

In summary, the final structure of the Ag(I)-thiolate complex is not only affected by experiment and crystalline conditions such as solvents, pH, and temperature, under which they are prepared, but also considerably influenced by the steric effect of the substituents in the ligand, Ag(I)/ligand ratio, auxiliary or co-ligand, and counter anion of Ag(I). The impact of the types of the thiolate ligands to the structural characteristics of the Ag(I)-thiolate coordination polymers could be addressed. For example, using secondary or tertiary alkyl thiolate ligands, the silver ion is coordinated with two thiolate ligand molecules, leading to one dimensional zig-zag or double chain structure. Primary alkylthiolate ligands often lead to layered two dimensional structures with trigonal geometry of Ag atom, with side chains extending up and down on both sides of the layers. The involvement of N/P/O atoms thiolate ligand and co-ligand could result in higher coordination number of the metal ions thus more complexed polymer networks. Ag(I)···Ag(I) interactions represent a unique feature that lead to special structural characters and physical properties. Thiolate ligandscould bring together and strengthen the Ag(I)-Ag(I) contacts. Counteranions of Ag(I), coligands and solvents also play important roles in modulating the

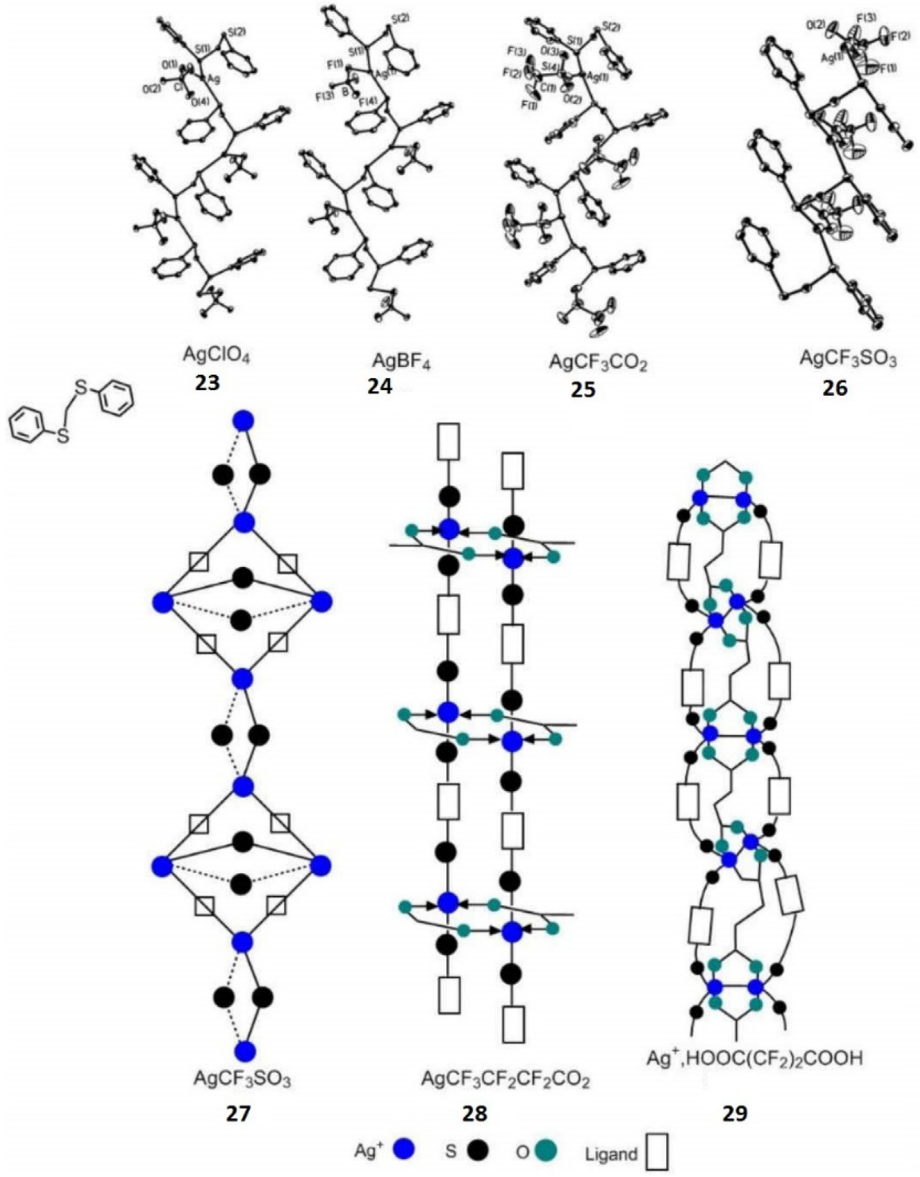

Fig. 9. Proposed structures of single chains in **23**–**26**, double-stranded chains of **27** and **28**, and 2D network of **29**. Reprinted with permission from Ref. [47].

Ag(I)-Ag(I) distances. Self-assembly of Ag(I)-thiolate complexes into supramolecular structures of more structural complexity can be promoted by the Ag(I)···Ag(I) interactions, mixed donor atom coordination and inter-side chain interactions. In 2D and 3D Ag (I)-thiolate coordination polymers with more structural rigidity and diversity, flexible electronic states of the Ag(I)-ligand complexes, Ag(I)···Ag(I) interactions and side chain interactions function together to generate unique physical properties. For example, Ag(I)···Ag(I) interactions have been found to contribute greatly to the thermal contraction and negative linear compressibility in crystallized silver complexes [47]. Photothermal effect is attributed to the intra-ligand or inter-ligand charge transfer and electron-hole recombination within confined Ag-S networks. Luminescent properties are determined by the LMCT processes [50,51] and can be strongly altered by the Ag(I)···Ag(I) interactions of the ligand-to-metal–metal charge transfer (LMMCT) nature [52,53]. Those physical properties therefore afford great potentials for sensing applications.

3. Ag(I)-thiolate coordination polymers as physical sensors

The conformational and coordination flexibility of the Ag(I)-thiolate coordination polymers make them sensitive to external physical stimuli such as temperature, electricity, and light. In addition, the Ag(I)···Ag(I) interactions related unique luminescence properties from the LMCT or LMMCT state and the semiconductive features are significant for designing multifunctional physical sensors. By introducing mixed ligands or transition metal centers into the coordination polymers, the sensitivity and selectivity of these sensors can be further tuned. In this part, we will summarize several recent examples of the Ag(I)-thiolate coordination polymers for thermochromic and photothermal sensing. Despite the fact that Ag(I)-thiolate coordination polymers have been reported for their semiconductive properties, their applications as electrochromic or electrochemical sensors remain limited. Zhu's group reported highly crystalline films of a silver-thiolate coordination polymers $[Ag_5(C_6S_6)]_n$ with an electrical conductivity up to 250 S·cm^{-1} at

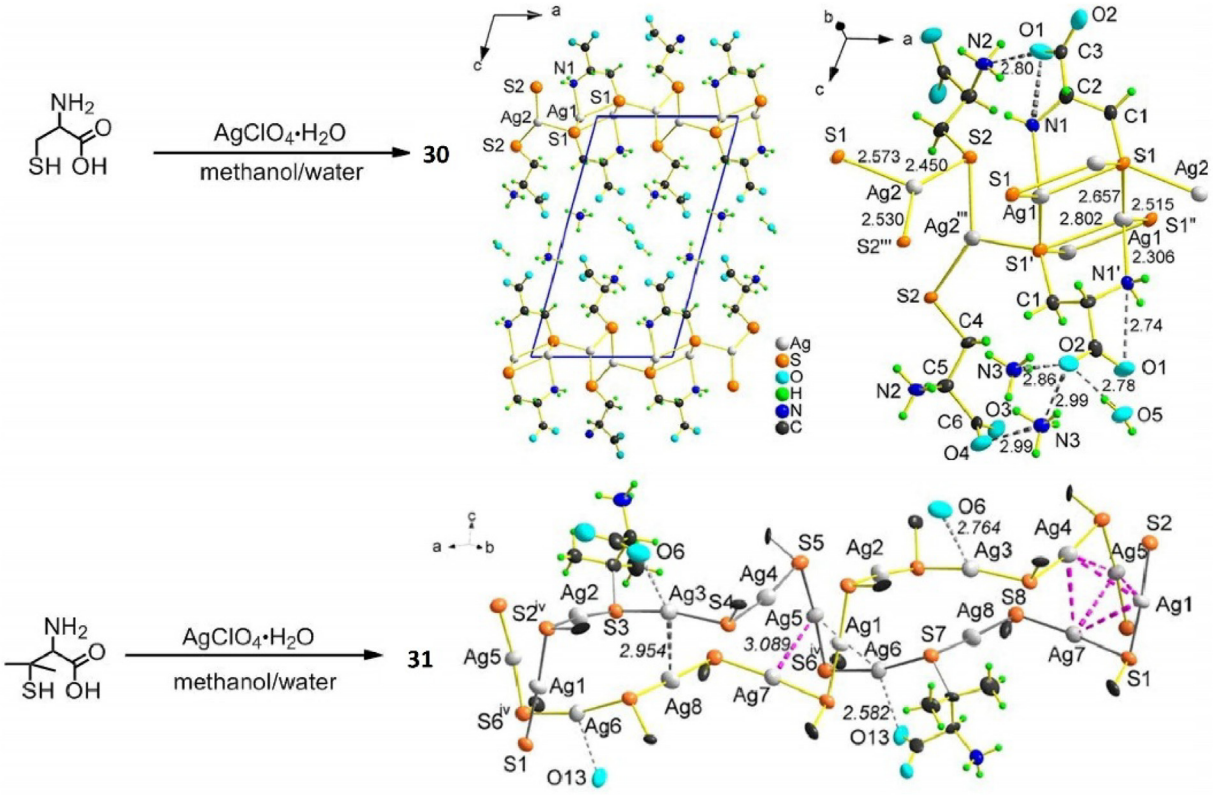

Fig. 10. (a) Layered structure of **30** with AgS_3N (Ag1) and AgS_3 (Ag2) unit in the *ab* plane and the structure is supported *via* hydrogen bonds that are shown as dashes lines between carboxylate oxygen O2 and O5 and N3, and (c) the crystal structure of **31**. Bond lengths are given in Å. Reprinted with permission from Ref. [49].

300 K [54]. Moreover, a much higher room-temperature conductivity of 7.3 × 10^{-2} S·cm^{-1} was discovered for $LiBHEt_3$ reduced $[Ag_5(C_6S_6)]_n$. Zang *et al.* [55] reported assembly of the Ag-S nanoclusters and rigid perfluorinated aromatic carboxylic acid (2,3,5,6-tetrafluorobenzene-1,4-dicarboxylate) into a silver-sulfur nanowire array. They observed an electrical conductivity of 1.01 × 10^{-8} S·cm^{-1} at room temperature. In that silver-sulfur nanowire array, Ag(I)···Ag(I) interactions along (1 0 0) direction of single crystal of nanowire are shown to play an important role for the conductivity. Thus, there remains great space to explore the Ag(I)-thiolate coordination polymers based electrochromic or electrochemical sensors.

3.1. Thermochromic sensing

Thermochroism is the property of a material to change its color due to changing in surrounding temperature. Traditional organic thermochromic sensors include thermochromatic liquid crystals and leuco dyes such as spirolactones, flurans, spiropyrans mixed with proton donor chemicals. After absorbing heat, the crystallic or molecular structure of the dyes undergo changes that leads to emission of changed wavelength [56]. The flexibility of the coordination of the Ag(I) with ligands and the Ag(I)···Ag(I) interactions open up new avenue for the Ag(I)-thiolate coordination polymers to undergo structural change upon temperature stimuli, which results for the charge transfer process in the ligands and between the ligands and Ag(I), and thereby changes in the luminescence properties. Temperature-induced conformational change of the Ag(I)-thiolate coordination polymers has been shown to lead to changes in the photophysical properties. Mak *et al.* [57] reported reversible transformation of tetragonal $[(Ag_{12}(SBu^t)_8(CF_3COO)_4(bpy)_4)]_n$ (**32**) (bpy = 4,4′-bipyridine) into trigonal $[(Ag_{12}(SBu^t)_8(CF_3COO)_6(bpy)_3)\cdot(DMAc_x\cdot toluene_y)]_n$ (**33**) using solvent at room temperature (Fig. 11). Singly emissive tetragonal **32** with disconnected D_{2d} 5–2-5 arrangement of the Ag_{12} cores transforms to trigonal dual emissive **33** with a C_{3v} cuboctahedron arrangement, resulting in shrinking nearly half of the thickness along the *c*-axis. **33** displays dual emission, at 463 nm assigned to the π,π* triplet state of bpy ligands with a lifetime of 10.1 ms at 83 K and 620 nm assigned to the triplet states in dodenuclear Ag-S cluster of LMMCT mixed with metal-centered states with a lifetime of 85.5 μs at the same temperature. The dual emission is highly sensitive to excitation energy and temperature. For **32**, dual possible transitions of different energies were observed, with an excitation maximum at 365 nm with a shoulder at 338 nm at 83 K. The low energy excitation at 365 nm arises from the inter-ligand *trans*-metallic charge-transfer (ITCT, S/Ag → bpy) and the high energy excitation at 338 nm arises from the LMMCT (S → Ag) mixed with metal center transition. Single emission at 507 nm with a lifetime of 12.35 μs was observed. Silver core shrinkage from Ag(I)···Ag(I) interactions in the **33** is associated with the energy level of LUMO that is lower than that of bpy centers, rendering two emissive centers locating on the silver clusters and the bpy linkers, respectively. Furthermore, bpy-NH_2 was introduced as a mixed-ligand resulting in thermochromic **33**/NH_2 to increase the blue emission component and the dichromatic core–shell **33@33**/NH_2. Both of them were applied for thermochromic sensing. Linear relationship of temperature to the emission intensity ratio was established in the range of 83–233 K, with a sensitivity of 0.347% K^{-1}. A rational design of Ag(I)-thiolate coordination polymers for dual-emissive thermochromic sensing by creating highly temperature-dependent cluster chromophores is shown operative.

Veselska *et al.* [58] reported crystal structures of lamellar $[Ag(p\text{-}SPhCO_2H)]_n$ (**34**) and $[Ag(p\text{-}SPhCO_2Me)]_n$ (**35**), synthesized with distorted Ag_3S_3 honeycomb networks separated by non-interpenetrating thiolate ligands and herringbone packing, and

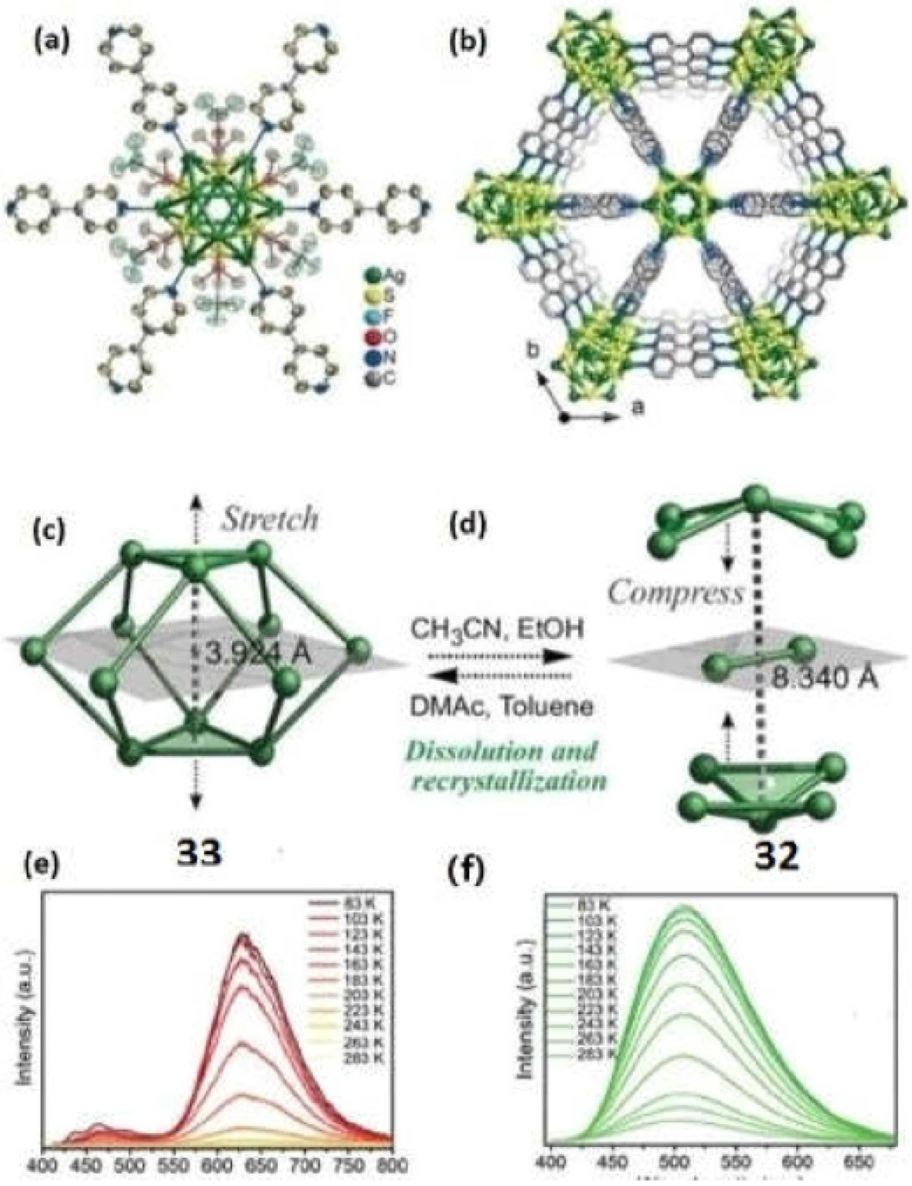

Fig. 11. (a, b) Perspective view of $Ag_{12}S_6$ node with six pendent bpy linkers and stacking of 2D network structure of **32**; (c, d) Comparison of Ag_{12} core structures in **33** and **32.** (e, f) Emission spectra of **33** and **32**, respectively. Reprinted with permission from Ref. [57].

applied them for thermochromic sensing. **34** and **35** both display thermochromic luminescent response in the solid state, with λ_{ex} = 380 nm and λ_{em} = 700 nm at 273 K for **34** and λ_{ex} = 368 nm and λ_{em} = 580 nm at 243 K for **35.** At lower temperature of 93 K, excitation and emissions are shifted to higher energies, with λ_{ex} = 352 nm and λ_{em} = 484/528 nm for **34** and λ_{ex} = 364 nm and λ_{em} = 489/526 nm for **35** (Fig. 12). The blue-shifted excitation and emission at lower temperature are attributed to the enhanced rigidity of the network that reduces the energy loss from non-radiation decay. For **34**, excitation at 220–340 nm results in emission at high energy while excitation at 360 nm, lower energy emission was observed. For **35** excitation at 220–360 nm result in both high energy emissions and low energy emission (650 nm) while from λ_{ex} = 380 nm, low energy emission at 700 nm was observed. The excitation wavelength dependent emission that is opposite to classical photophysics is explained by the anti-Kasha's rule of a decrease in the number of excited-states at decreased excitation energy. The emission in the high energy range originates from the ligand-centered $^3\pi\pi^*$ transition while in the low energy range from the LMCT state.

3.2. Photothermal sensing

Photothermal effect is produced by the excitation of a material that results in thermal energy, which is an emerging field in cancer therapy, sustainable and efficient energy. Inorganic materials including graphene, carbon nanotubes and transition metal nanoparticles have been reported as classical photothermal materials for temperature sensing, water evaporation and solar steam evaporation [59]. By employing small organic photosensitizers such as porphyrin and indocyanine green in conjugation with polymer nanoparticles, photothermal therapy agents of excellent biocompatibility for cancer therapy have been achieved [60]. Theoretically, photothermal effect originates from nonradiative electron-hole recombination, which depends largely on the phonon dispersion and electron–phonon coupling in the material.

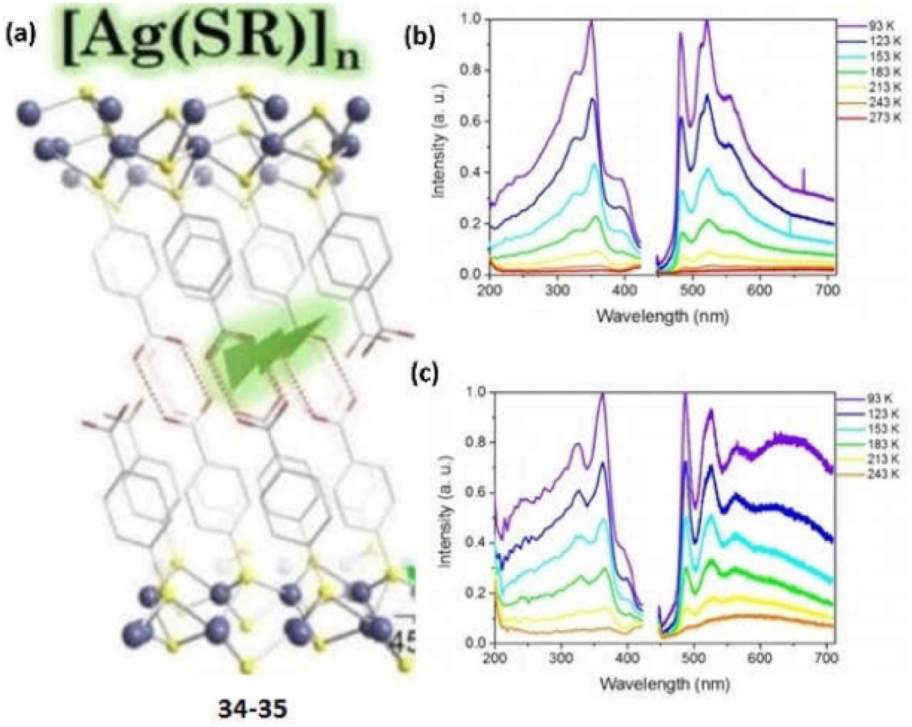

Fig. 12. (a) Structure of lamellar silver thiolate coordination polymer **34** and **35**. (b, c) Excitation and emission spectra of **34** and **35**, respectively. Reprinted with permission from Ref. [58].

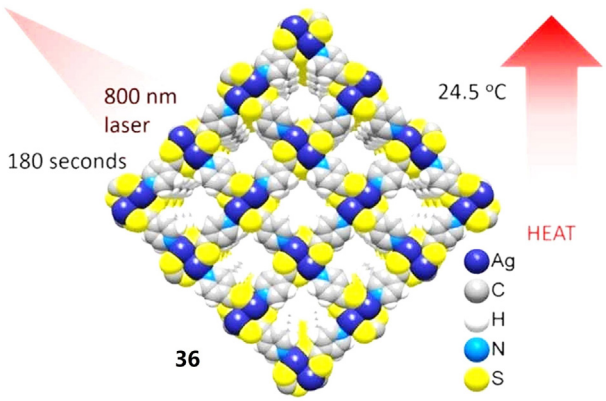

Fig. 13. Structure and photothermal effect of lamellar silver thiolate coordination polymer **36**. Reprinted with permission from Ref. [61].

Higher polarizability, higher electron effective mass and easier/faster polaronic reconstruction of charge carriers lead to stronger trend of polaronic reconstruction thus more nonradiative electron-hole recombination [61]. Applications of Ag(I)-thiolate coordination polymers in photothermal sensing represent a relatively new subject of promising future potentials. Near-infrared photothermal effect was achieved in 2-dimentional coordination polymer **36** from Ag(I) and pyridine-4-dithiocarboxylate (Py-4-CSS) (Fig. 13). Single crystal X-ray diffraction analysis reveals a layered structure in which each Ag^+ coordinates to two sulfur atoms and one nitrogen atom to generate a "T" shaped [AgS_2N] fragment [61]. Ag(I)···Ag(I) interactions of 3.04 Å distance are discovered in dimers which are bridged by four Py-4-CSS ligands in the *ab* plane. The layers of **36** stack in an ABAB relation along *c* axis, leading to one-dimensional cylindrical pores, in which pyridine rings stack in head-to-tail fashion along the *c* axis. The proper orientation of the pyridine rings allows optimal π-π interactions that contribute to the interlayer charge transport. Under 800 nm radiation, the temperature of the coordination polymer raised up with a maximum increase by 24.5 °C in 3 min at a photothermal conversion efficiency of 22.1%, 2 times that of pure inorganic Ag_2S materials, which is among the inorganic materials of highest efficiency. The coordinating nitrogen atoms in the pyridine moieties are critical in promoting the charge transfer between the dithiocarboxylate ligands. Large dielectric constant and flat energy bands were obtained, indicating that the coordination polymers have a high electron effective mass and are easy to conduct nonradiative electron-hole recombination, giving off heat.

4. Ag(I)-thiolate coordination polymers as chemosensors

The prosperous developments of the silver-thiolate coordination chemistry have tremendously promoted the applications of Ag(I)-thiolate coordination polymers as chemosensors for ions [62–65], thiols [66–71], VOCs [18], saccharides [72] and explosives [73]. Moreover, silver-thiolate coordination complexes are also employed to creating hydrogels [74–80]. The designing strategies of the Ag(I)-thiolate coordination polymers as chemosensors mainly are: (i) rationally equipping the thiolate ligand with binding groups towards given analyte, which upon binding triggers sensitive structural and/or spectral changes; (ii) changing the composition of ligand and metal ions that photophysical properties of the formed coordination polymers could be altered; (iii) *in situ* generating chromophores relating to the argentophilic interactions upon the formation of Ag(I)-thiolate coordination polymers, with unique luminescent properties of no spectral background; (iv) introducing multiple interaction motifs or co-polymerization with other ligands, to allow multivalent interactions and thereby signal amplification. As sensory ensembles, Ag(I)-thiolate coordination polymers have shown detection limits of sub-μM to pM level, together with high selectivity, and have therefore demonstrated

excellent sensing performance among the recently reported chemosensors [81–83]. Applications for three typical kinds of analytes are presented.

4.1. Metal ions sensing

It has been reported that Ag(I)-cysteine [66] or Ag(I)-GSH [75] coordination polymers of LMMCT excited-state are weakly fluorescent. Jiang *et al.* [62] reported a facile method to enhance the LMMCT fluorescence by the decorating the cysteine ligand with a naphthalene moiety (NCys, **37**) as an antenna to harvest light for exciting the coordination polymers (Fig. 14). Inserting a naphthyl fluorophore in the cysteine ligand creates both the π–π stacking in the Ag(I)-NCys coordination polymers and an energy transfer pathway for dual emission at 337 nm and 441 nm under the excitation at 283 nm for naphthyl moiety. When Ag^+ was added into the solution of **37**, Ag(I)-**37** coordination polymer formed with the aid of the argentophilic interaction, leading to the quenching of fluorescence at 337 nm while the developing of a new emission at 441 nm, assigned to the LMMCT from the thiol ligand to the silver chain. This strategy is applicable for Ag^+ at sub-μM concentration level and, in particular, the response is specific to Ag^+ among other highly interfering ions such as Hg^{2+} and Ba^{2+}, demonstrating nicely the significant role of argentophilic interactions in promoting the formation of the coordination polymers that afford signal amplification and thereby highly specific recognition of Ag^+. This example demonstrates that by rationally designing the thiolate ligand, the luminescence property could be modulated, adding new merit of fluorescent sensing using the Ag(I)-thiolate coordination polymers.

Replacing Ag^+ in the Ag(I)-thiolate coordination polymers by Hg^{2+}, the resultant photophysical changes are taken for the sensing of Hg^{2+}. Li *et al.* [64] devised a network of Ag^+ (**38**) with sulfhydryl-functionalized carbon dots for Hg^{2+} sensing (Fig. 15). Fluorescence of **38** is significantly quenched by Ag^+ and recovered upon the addition of Hg^{2+}. Fluorescence intensity varies linearly with Hg^{2+} concentration over 0.01–0.75 nM, exhibiting an extremely low detection limit (LOD) of 4.2 pM. The formation of amalgam Ag_2Hg_3 effectively prevents the re-quenching of the fluorescence by free Ag^+ and Hg^{2+}, which also guarantees a credible evaluation of the emission.

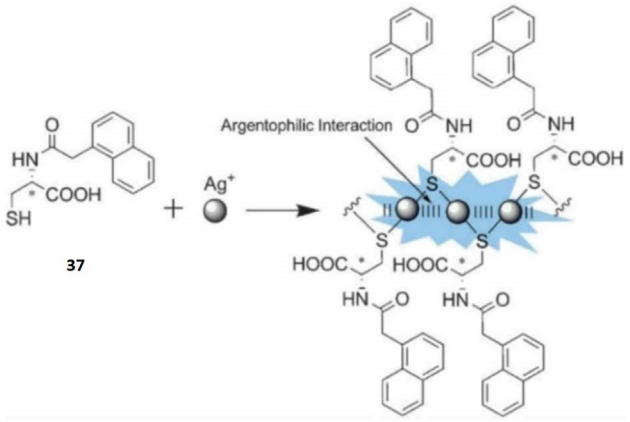

Fig. 14. Formation of Ag(I)-**37** coordination polymer in 1:1 (v/v) EtOH-H_2O containing 5 mM NaAc-HAc buffer of pH 5.0 and enhanced LMMCT fluorescence for sensing Ag^+. Reprinted with permission from Ref. [62].

4.2. VOCs and gas sensing

The sensing of small gaseous molecules is very important in industry, medical and biological research, and environmental monitoring. The stability and photophysical properties of metal clusters have been considered largely dependent on their core, ligands and environments. While the inherent instability and poor room-temperature luminescence quantum yields of silver chalcogenide clusters (SCC) has hampered extensive study of their potential applications. Mak *et al.* [18] developed a luminescent dodecanuclear silver cluster based MOF **39** of enhanced stability *via* reaction of AgS^tBu with CF_3COOAg and rigid bidentate bridging ligand bpy in a mixed solvent of CH_3CN and C_2H_5OH (Fig. 16), remaining stable from minutes to one year, with about a 60-fold increase in the luminescence quantum yield. The luminescence of this MOF originates from a metal Ag(I)-to-ligand (bpy) (MLCT) excited state with mixing from the ligand (S,O)-to-ligand (bpy) (LLCT) character. The long lifetime of **39** of 0.20 μs at microsecond scale indicates the triplet nature of the excited state. Photoluminescence of is switched off by air/O_2 quickly in less than 1 sec, with a quenching rate constant *kq* for O_2 of 3.2×10^6 kPa^{-1} s^{-1} and a LOD defined by 1% quenching of 32 Pa. This high performance of O_2 sensing in the solid-state is attributed to (a) the interaction of O_2 with the exposed bpy linkers that correlate with its LUMO, that the triplet energy is transferred and its emission is quenched, and (b) the fully openness of the MOF pores allow O_2 to freely permeate and diffuse in the channels to effectively collide with the chromophores thus quickly quench the emission. The quenched luminescence of **39** is instantly restored by the presence of various VOCs, exhibiting different color emission from green to yellow-orange at room temperature, **39** being therefore an ultrafast dual-functional chemosensor for air/O_2 and VOCs.

Zang *et al.* [84] reported a flexible pillared-layered silver-chalcogenolate cluster based metal–organic framework **40**, from reaction of CF_3COOAg and AgS^tBu with 4,4′-bipyridine, and multidentate phenylphosphonic acid ($PhPO_3H_2$) ligand as a functional hydrogen-bond donor. **40** allows for an effective distinguishing of chloromethanes, CH_2Cl_2, $CHCl_3$, and CCl_4, by adsorption-induced dynamic gate opening process, in a solvatochromism manner (Fig. 17). Fluorescence emission of **40** at 518 nm remains unchanged after adsorbing CH_2Cl_2, but shifted to red by 15 nm and 52 nm when CCl_4 and $CHCl_3$ are respectively introduced. The

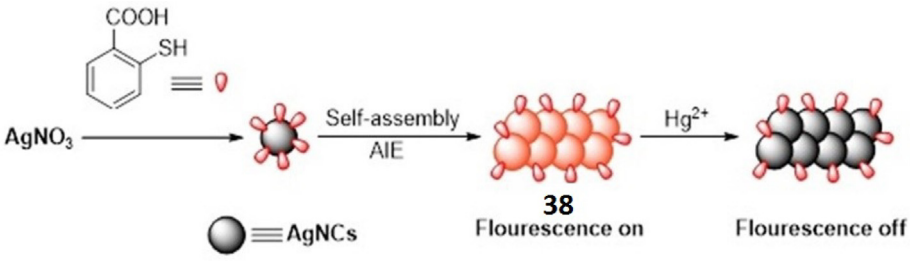

Fig. 15. Schematic illustration of the self-assembly of AgNPs **38** with AIE and the fluorescence quenching of AgNPs **38** in the presence of Hg^{2+}. Reprinted with permission from Ref. [64].

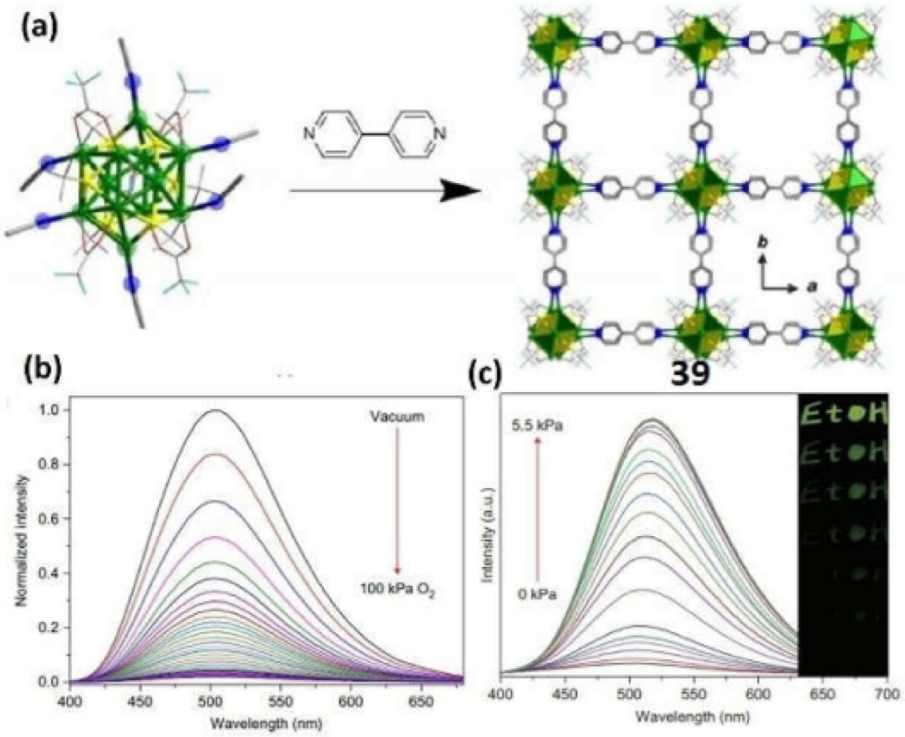

Fig. 16. (a) Synthesis and crystal structure of **39** viewed along the *c*-axis. (b, c) Emission spectra of **39** toward different partial pressures of O_2 and EtOH, respectively. Reprinted with permission from Ref. [18].

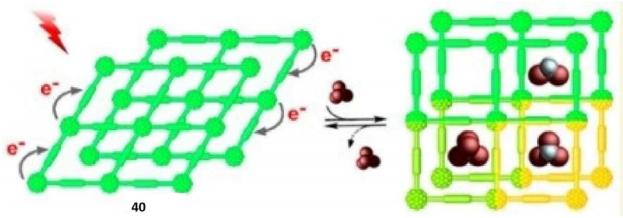

Fig. 17. Schematic illustration of chloromethane-induced change of fluorescence of **40**. Reprinted with permission from Ref. [84].

change of fluorescence from green to yellow is readily seen by naked eyes. Surprisingly, this tendency of luminescence response of these chloromethanes are deviated from the trend of the dielectric constant and polarity order of the solvents, CH_2Cl_2 > $CHCl_3$ > CCl_4. The changes of fluorescence are ascribed to the relative orientations of the dipole moment vector of the chloromethane molecules towards bpy linkers, which influents the intermolecular charge transfer transition.

4.3. Amino acids and saccharides sensing

Thiols are important for human lives. For example, the abnormal glutathione level will increase the risks of certain cancers and heart diseases. Benefiting from the metallophilicity related characteristic absorption and photoluminescence properties of the M(I)-thiolate coordination polymers, Jiang *et al.* [66] envisaged that the *in situ* formed Ag(I)-thiolate coordination polymers could act as a feasible sensing ensemble. Ag(I)-cysteine (Cys) coordination polymers were developed as sensing ensembles for detecting and discriminating L- and D-cysteine (Fig. 18). In the presence of

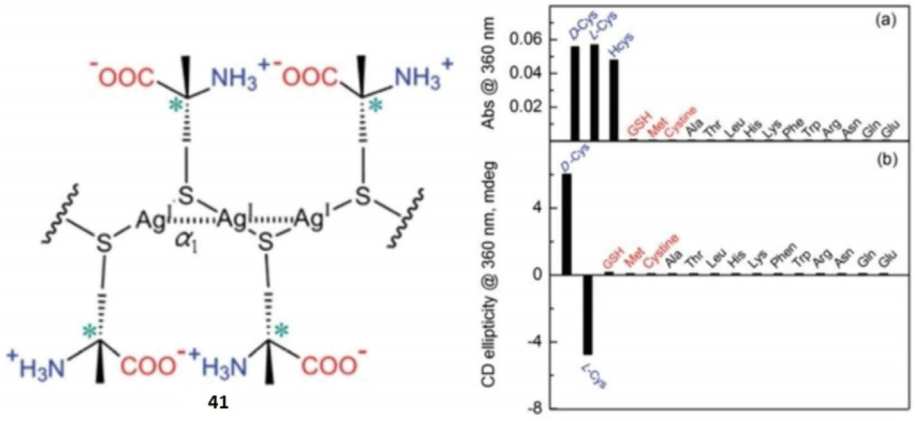

Fig. 18. *In situ* formation of Ag(I)-cysteine (Cys) coordination polymer **41** as sensing ensemble to detect and discriminate L- and D-cysteine. Reprinted with permission from Ref. [66].

Ag^+ and Cys, Ag(I)-Cys coordination polymers **41** are formed, exhibiting characteristic absorption and mirror imaged CD signals at 280 nm and 360 nm, relating to the LMMCT state. By employing this method, cysteine was recognized over 14 other thiols, demonstrating therefore the high selectivity of the sensing scheme. It is worthy pointing out that, despite the chiral center in cysteine is one $-CH_2-$ away from the coordinating S atom, strong splitting CD signals were observed in the Ag(I)-Cys solution at wavelengths corresponding to the LMMCT absorption. This also shows the synergetic interplay of the electrostatic interaction the thiolate ligand side chains and the argentophilic attractions in the Ag(I)-Cys polymeric backbone, explaining the observation of transferred chirality from cysteine residue to the Ag(I)···Ag(I) polymeric backbone and the related chromophores, and thereby the CD signals. Yan *et al.* [85] reported sensing of L-cysteine based on self-assembly of chiral complex nanoparticles from Ag(I) and L-cysteine. Upon addition of 50 μM Ag(I) to 50 μM L-cysteine solution, new CD signals of two positive peaks at 210 and 300 nm, and three negative peaks at 250, 280 and 360 nm appeared, which turned into an S-shaped signal with a negative peak at 290 nm and a positive peak at 254 nm after standing for 100 hr. As a CD probe for L-cysteine, this sensing scheme demonstrated a high selectivity at Ag(I) concentration of 5 μM for 5 μM L-cysteine over other 19 amino acids and 6 structurally related thiols at concentration of 500 μM, in that only L-cysteine shows an S-shaped signal in the range of 230–350 nm. The detection limit for L-cysteine is at the μM level. A possible binding model for initial complexation of Ag(I) to L-cysteine through S atom and weak bonding *via* O atoms was proposed and supported by the FTIR observation of the absence of the stretching vibrations at 2552 cm^{-1} of S-H and O–H at 1425 cm^{-1}, C-O at 1295 cm^{-1} and C-O–H at 1348 cm^{-1}. After standing for extended self-assembling of the chiral complex, an oligomeric structure was proposed to form with the help of the multiple N–H and C = O bonds in the self-complementary hydrogen bonding, N-H···O═C, which was supported by the simultaneous enhancement of the 1677 and 1566 cm^{-1} bands. The probe was applied for quantitative analysis of L-cysteine in human urine samples.

Based on the fact that the molecular chirality of chiral thiolate ligands is transferred and amplified upon the formation of coordination polymers, the potential of Ag(I)-thiolate coordination polymers as chiral sensing platform was inspired. Jiang *et al.* [72] further explored the chirality sensing of monosaccharides using a boronic acid functionalized achiral thiol ligand to form coordination polymers with Ag(I) (**42**), *p*-mercaptophenylboronic acid (MPBA), affording multiple boronic acid groups for binding chiral monosaccharides. The achiral coordination polymers were expected to and indeed turn into CD active upon the addition of chiral monosaccharide that binds to the boronic acid group(s) on the polymeric backbone (Fig. 19), exhibiting monosaccharide identity dependent CD profile and thus allowing identification of the chiral saccharide species. It was suggested that by introducing additional interaction motifs such as the N → B interaction or *via* co-polymerization of another thiol ligand, multivalent interactions could be made possible for extended chiral sensing.

5. Ag(I)-thiolate coordination polymers as multifunctional hydrogels.

Thiol-containing molecules have been proved to form hydrogels upon binding with coinage metal cations such as Au(I), Ag(I) and Cu(I) *via* self-assembling into supramolecular metal-thiolate polymers that are stabilized by metallophilic interactions [86–88]. GSH was the first reported to form hydrogel upon interacting with gold (I) that the aurophilic interactions are functioning [89]. It was later reported to form the Ag(I)-glutathione hydrogels under acidic conditions [75]. This supramolecular hydrogel releasing the captured

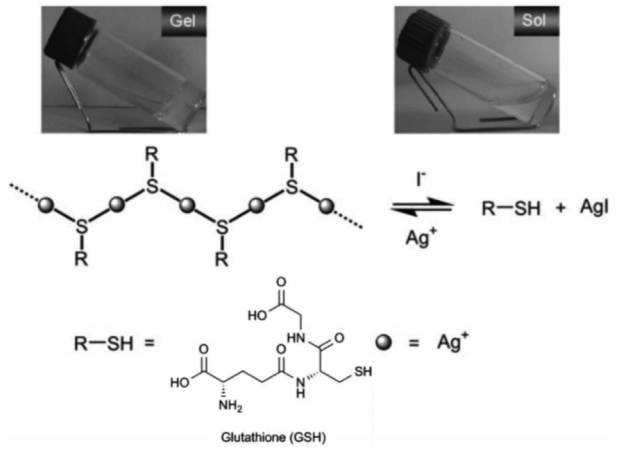

Fig. 20. Reversible gel-sol transition of Ag^+-GSH hydrogel triggered by the addition of I^- into hydrogel and subsequent Ag^+ into sol solution. Reprinted with permission from Ref. [75].

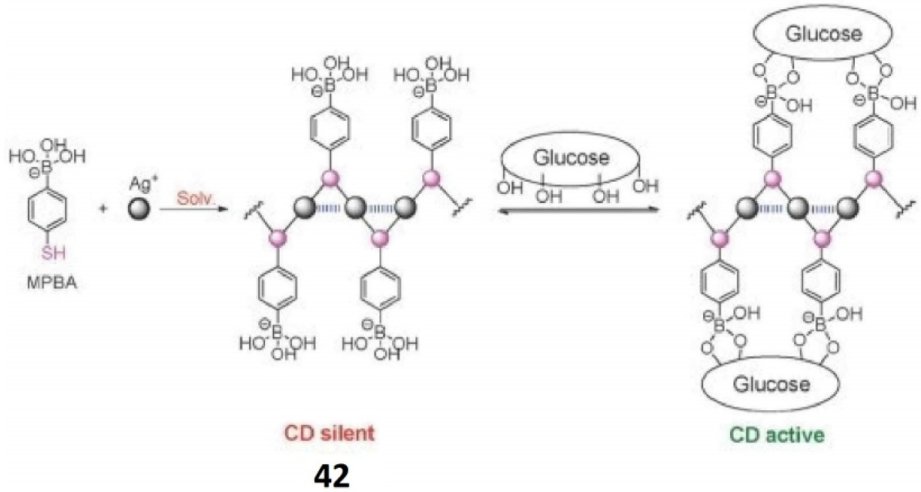

Fig. 19. Chirality sensing of glucose by achiral Ag(I)-MPBA coordination polymer **42**. Reprinted with permission from Ref. [72].

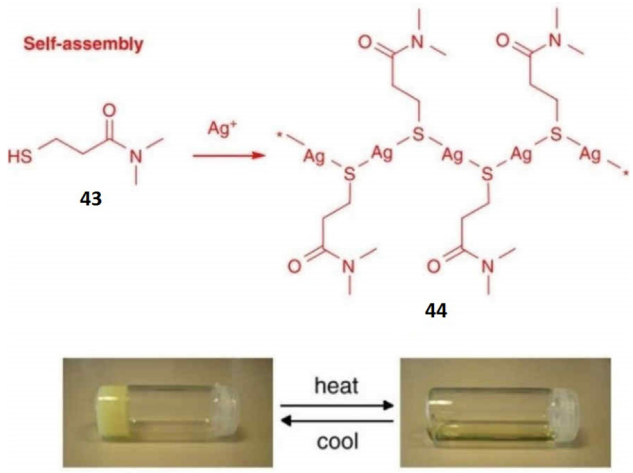

Fig. 21. Thermo-responsive transition of argentophilic hydrogel **44**. Reprinted with permission from Ref. [74].

water that is much more than the introduced I^-, capable of selectively recognizing I^- by a pronounced gel-sol phase transition (Fig. 20). It is highly selective that other halogen anion (F^-, Cl^-, and Br^-) or $H_2PO_4^-$ does not lead to such a phase transition and therefore allows a facile and visual approach for recognition of I^- *via* naked eyes.

Odriozola *et al.* [74] reported an argentophilic hydrogel **44** that exhibits temperature-sensitive properties (Fig. 21). The hydrogel becomes clear when temperature is raised to its gel melting temperature (T_{gel}), while the subsequent cooling of this sol solution leads to a reversible sol-to-gel transition. The value of T_{gel} closely relates to the concentration of thiol ligand **43**, which establishes an efficient way of controlling the thermo-responsive property of the hydrogel **44**.

Many ultrashort peptide sequences as short as di- or tripeptides have shown to self-assemble into hydrogels with endogenic biocompatibility and biodegradability [90,91]. Grande *et al.* [78] developed neutral metallophilic hydrogels by tuning the isoelectric point (pI) of the terminal amine protected di- and tripeptides containing cysteine (Cys, C), arginine (Arg, R) and glycine (Gly, G) residues. The strong basicity of guanidinium group of Arg residue (pKa = 12.5) increases the final pI of the peptides at around physiological pH. All of the four terminal amine acetylated peptides (CR, RC, RGC, RCG) form pH- and thermo-reversible hydrogels with Ag(I) and Au(I) at 3 wt%. Odriozola *et al.* [76] investigated structure-dependent morphologies and phase-transitions of silver-thiol hydrogels by using thiol ligands **45**–**49** (Fig. 22). The hydrogels built from neutral thiols **45**–**47** are opaque with fibril microstructures. However, acidic thiols **48**–**49** give transparent hydrogels in a sheet-like microstructures. Moreover, the hydrogels from thiols **45**, **47**, **48**, and **49** are thermo-reversible that undergo temperature-driven phase transitions, while hydrogel from thiol **46** remains in gel phase even at the boiling point of water. MALDI-TOF MS and size exclusion chromatography analysis indicate that the neutral hydrogels are composed of tetrameric species, whereas the acidic hydrogels are composed of slightly larger oligomers (n = 8–14). These researches open up a new avenue towards developing thiol containing new hydrogelators, spanning from the first reported cysteine-containing peptides to thiol-modified synthetic molecules.

Agomir874 is a type of miRNA from miRNA874 that regulates expression of matrix metalloproteinases (MMPs) of the tissue extracellular matrix (ECM) in nucleus pulpous (NP) that may relate to the development of intervertebral disk degeneration (IVDD) [92,93]. Chen *et al.* [80] investigated Ag-$(PEGSH)_4$ hydrogels for potential application as miRNA delivering materials by loading into Agomir874 and *in situ* injection into the degenerative intervertebral disk (Fig. 23). The hydrogels are injectable, self-healing, antimicrobial, degradable, and favorable for Agomir loading. Mechanical characterizations show that the hydrogel is similar to normal intervertebral disk and can match and compensate for the elasticity of degenerated intervertebral disk. The reversible bond breaking of Ag-SR under shear force turns hydrogel into injectable fluid, which later reforms the hydrogel after injection. Agomir874 is thereby shown to down-regulate the expression of

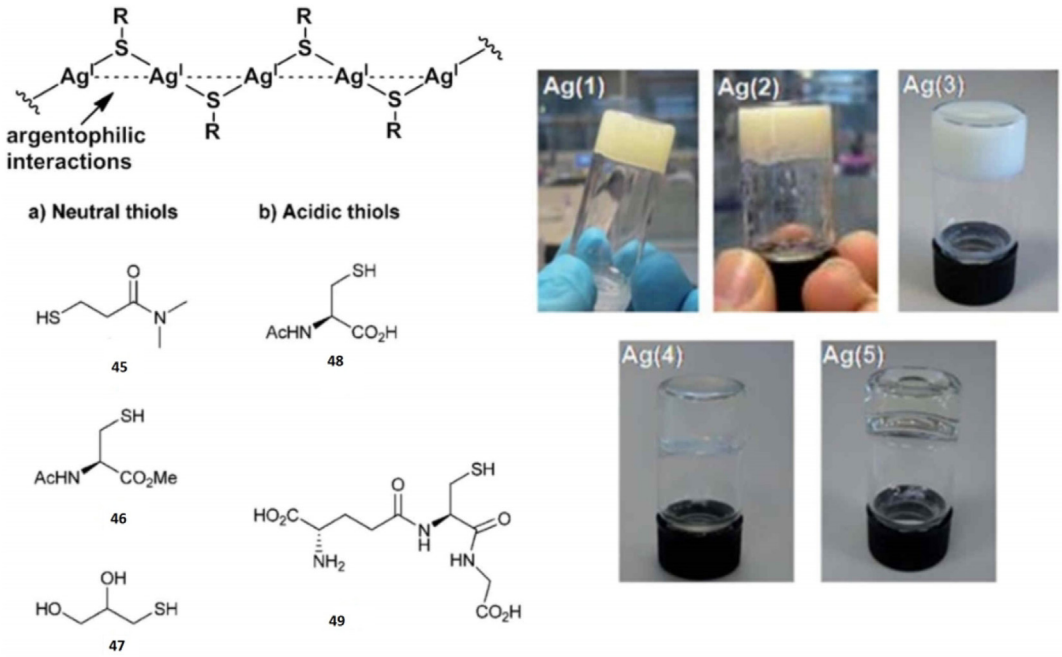

Fig. 22. Construction of neutral opaque and acidic transparent argentophilic hydrogels by coordination of Ag^+ with thiol ligands **45**–**49**. Reprinted with permission from Ref. [76].

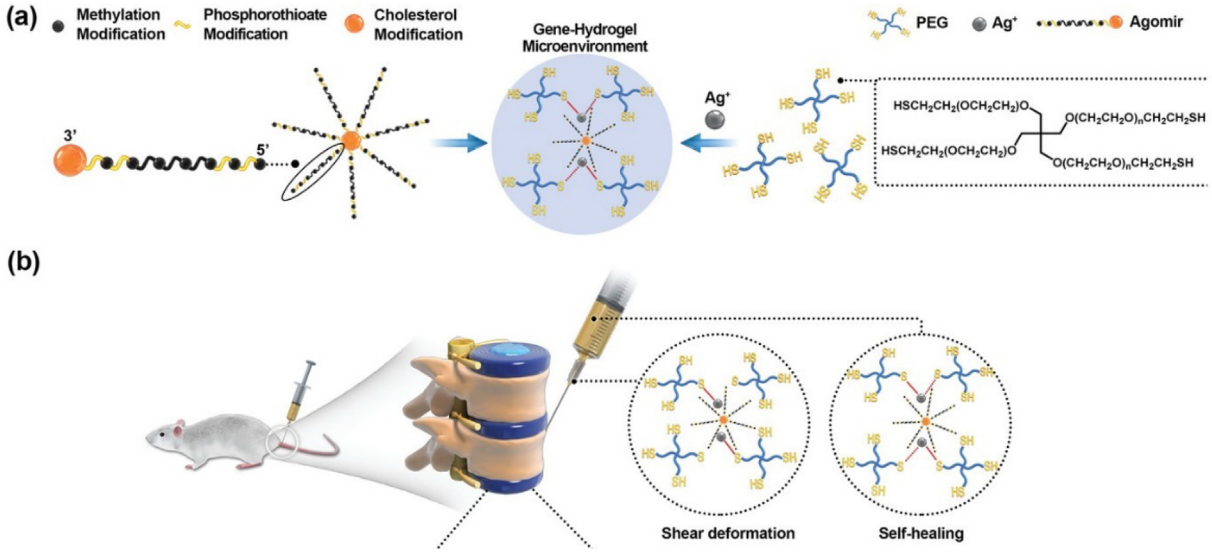

Fig. 23. Schematic representation of gene-hydrogel microenvironment for regeneration of IVDD through Ag-$(PEGSH)_4$ hydrogels. (a) Formation of gene-hydrogel. (b) The Agomir loaded hydrogels were injected into the intervertebral space to build the gene-hydrogel microenvironment. Reprinted with permission from Ref. [80].

MMPs, regulating the metabolism balance of ECM in NP and slowing the process of IVDD. The potential of Ag-$(PEGSH)_4$ hydrogels as biomaterials to deliver Agomirs is therefore confirmed

6. Conclusions

In this review, we summarized the synthesis, structures and applications of Ag(I)-thiolate coordination polymers as sensory ensembles. Synthesis and structures of Ag(I)-thiolate coordination polymers of diverse structures from 1D to 3D are presented according to the types of the substituents (R) in the thiolate ligand RSH. Properties of the Ag(I)-thiolate based coordination polymers, semiconductivity, luminescence, photothermal and thermochromic effects, are also discussed. Recent developments of physical and chemical sensors using the Ag(I)-thiolate coordination polymers and their hydrogels are reviewed. Particularly, as weak interactions including the argentophilic interaction that hold the coordination polymers are sensitive to the external stimuli and analyte binding, they do have been successfully employed to establish unique sensing schemes of good performance in terms of high sensitivity and selectivity.

The advantages of Ag(I)-thiolate coordination polymers as sensory ensembles include the ease of synthesis of both the ligand and the polymers and the structural diversity of the supramolecular assembly. The cooperative weak interaction network operating to stabilize the coordination polymers affords signal amplification that could lead to enhanced sensing performance. The *in situ* generated chromophores relating to the argentophillic attractions in the polymeric backbone allows background free spectral sensing while the spectral signal can be switched on and off subject to external conditions. While the disadvantages of these polymers mainly includes the limited types sensing species available up to date and the possible instability of the polymers in sensing in complicated biological systems. New thiol ligands need to be developed for more complicated sensing. Current applications for sensing following the strategy remain in the early stage and their sensing performance have not well related to the diverse structures of the available Ag(I)-thiolate coordination polymers. Those vast structures deserve future attention for guiding the rational designing of the sensory systems and we believe those efforts would be rewarding.

Declaration of Competing Interest

The authors declare that they have no known competing financial interests or personal relationships that could have appeared to influence the work reported in this paper.

Acknowledgement

We gratefully appreciate the support by the NSF of China (grants 21435003, 91427304, 91856118, 21521004, 21904111, 21820102006, and J1310024), the Program for Changjiang Scholars and Innovative Research Team in University, administrated by the MOE of China (grant IRT13036), the S&T project of Xiamen (3502Z20203025), and Xiamen University Presidential Foundation (grants 20720170088 and 20720180023).

References

[1] K.M. Fromm, Nat. Chem. 3 (2011) 178.
[2] S. Eckhardt, P.S. Brunetto, J. Gagnon, M. Priebe, B. Giese, K.M. Fromm, Chem. Rev. 113 (2013) 4708–4754.
[3] M. Bosetti, A. Massè, E. Tobin, M. Cannas, Biomaterials 23 (2002) 887–892.
[4] D. Venkataraman, Y. Du, S.R. Wilson, K.A. Hirsch, P. Zhang, J.S. Moore, J. Chem. Edu. 74 (1997) 915.
[5] P. Wu, D.W. Grainger, Biomaterials 27 (2006) 2450–2467.
[6] H. Häkkinen, Nat. Chem. 4 (2012) 443.
[7] R. Jin, C. Zeng, M. Zhou, Y. Chen, Chem. Rev. 116 (2016) 10346–10413.
[8] J.F. Corrigan, O. Fuhr, D. Fenske, Adv. Mater. 21 (2009) 1867–1871.
[9] O. Fuhr, S. Dehnen, D. Fenske, Chem. Soc. Rev. 42 (2013) 1871–1906.
[10] B. Krebs, G. Henkel, Angew. Chem. Int. Ed. 30 (1991) 769–788.
[11] A.N. Khlobystov, A.J. Blake, N.R. Champness, D.A. Lemenovskii, A.G. Majouga, N. V. Zyk, M. Schröder, Coord. Chem. Rev. 222 (2001) 155–192.
[12] Q. Zheng, S. Borsley, G.S. Nichol, F. Duarte, S.L. Cockroft, Angew. Chem. Int. Ed. 58 (2019) 12617–12623.
[13] A. Aliprandi, D. Genovese, M. Mauro, L. De Cola, Chem. Lett. 44 (2015) 1152–1169.
[14] Q. Zhang, Q. Wang, X.-X. Chen, P. Zhang, C.-F. Ding, Z. Li, Y.-B. Jiang, Trends Anal. Chem. 109 (2018) 32–42.
[15] J.J. Vittal, Coord. Chem. Rev. 251 (2007) 1781–1795.
[16] H. Furukawa, K.E. Cordova, M. O'Keeffe, O.M. Yaghi, Science 341 (2013).
[17] S. Kitagawa, R. Kitaura, S.i. Noro, Angew. Chem. Int. Ed. 43 (2004) 2334–2375.
[18] R.-W. Huang, Y.-S. Wei, X.-Y. Dong, X.-H. Wu, C.-X. Du, S.-Q. Zang, T.C.W. Mak, Nat. Chem. 9 (2017) 689–697.
[19] A.Y. Robin, K.M. Fromm, Coord. Chem. Rev. 250 (2006) 2127–2157.
[20] V.W.-W. Yam, V.K.-M. Au, S.Y.-L. Leung, Chem. Rev. 115 (2015) 7589–7728.
[21] D.-L. Ma, V.P.-Y. Ma, D.S.-H. Chan, K.-H. Leung, H.-Z. He, C.-H. Leung, Coord. Chem. Rev. 256 (2012) 3087–3113.

[22] V. Bonačić-Koutecký, A. Kulesza, L. Gell, R. Mitrić, R. Antoine, F. Bertorelle, R. Hamouda, D. Rayane, M. Broyer, T. Tabarin, Phys. Chem. Chem. Phys. 14 (2012) 9282–9290.
[23] B.H. Lipshutz, Y. Yamamoto, Chem. Rev. 108 (2008) 2793–2795.
[24] S. Singha, D. Kim, H. Seo, S.W. Cho, K.H. Ahn, Chem. Soc. Rev. 44 (2015) 4367–4399.
[25] Z. Luo, K. Zheng, J. Xie, Chem. Commun. 50 (2014) 5143–5155.
[26] C.N. Lok, T. Zou, J.J. Zhang, I.W.S. Lin, C.M. Che, Adv. Mater. 26 (2014) 5550–5557.
[27] C. You, C. Han, X. Wang, Y. Zheng, Q. Li, X. Hu, H. Sun, Mol. Biol. Rep. 39 (2012) 9193–9201.
[28] O. Veselska, A. Demessence, Coord. Chem. Rev. 355 (2018) 240–270.
[29] S. Åkerström, Acta Chem. Scand. 18 (1964) 1308.
[30] H.G. Fijolek, J.R. Grohal, J.L. Sample, M.J. Natan, Inorg. Chem. 36 (1997) 622–628.
[31] F. Bensebaa, T.H. Ellis, E. Kruus, R. Voicu, Y. Zhou, Langmuir 14 (1998) 6579–6587.
[32] A. Parikh, S. Gillmor, J. Beers, K. Beardmore, R. Cutts, B. Swanson, J. Phys. Chem. B 103 (1999) 2850–2861.
[33] I.G. Dance, L.J. Fitzpatrick, A.D. Rae, M.L. Scudder, Inorg. Chem. 22 (1983) 3785–3788.
[34] S. Hong, A. Olin, R. Hesse, Acta Chem. Scand. A 29 (1975) 583–589.
[35] I.G. Dance, L.J. Fitzpatrick, D.C. Craig, M.L. Scudder, Inorg. Chem. 28 (1989) 1853–1861.
[36] I. Lindqvist, Acts. Cryst. 10 (1957) 29–32.
[37] W. Su, M. Hong, J. Weng, R. Cao, S. Lu, Angew. Chem. Int. Ed. 39 (2000) 2911–2914.
[38] D. Sun, G.-G. Luo, Q.-J. Xu, N. Zhang, Y.-C. Jin, H.-X. Zhao, L.-R. Lin, R.-B. Huang, L.-S. Zheng, Inorg. Chem. Comm. 12 (2009) 782–784.
[39] X.-P. Kang, Y.-S. Hu, L.-H. Zhu, Z. An, Inorg. Chem. Comm. 29 (2013) 169–171.
[40] Z. Chen, L. Zhang, F. Liu, R. Wang, D. Sun, CrystEngComm 15 (2013) 8877–8880.
[41] G.K. Kole, K.V. Vivekananda, M. Kumar, R. Ganguly, S. Dey, V.K. Jain, CrystEngComm 17 (2015) 4367–4376.
[42] K. Tang, M. Aslam, E. Block, T. Nicholson, J. Zubieta, Inorg. Chem. 26 (1987) 1488–1497.
[43] J. Dilworth, J. Hu. Adv. Inorg. Chem.: Elsevier (1993) 411–459.
[44] E. Block, M. Gernon, H. Kang, G. Ofori-Okai, J. Zubieta, Inorg. Chem. 28 (1989) 1263–1271.
[45] P. Perez-Lourido, J.A. Garcia-Vazquez, J. Romero, A. Sousa, E. Block, K.P. Maresca, J. Zubieta, Inorg. Chem. 38 (1999) 538–544.
[46] M.O. Awaleh, A. Badia, F. Brisse, Inorg. Chem. 46 (2007) 3185–3191.
[47] H. Schmidbaur, A. Schier, Angew. Chem. Int. Ed. 54 (2015) 746–784.
[48] M.O. Awaleh, A. Badia, F. Brisse, Cryst. Growth Des. 5 (2005) 1897–1906.
[49] B.O. Leung, F. Jalilehvand, V. Mah, M. Parvez, Q. Wu, Inorg. Chem. 52 (2013) 4593–4602.
[50] A. Barbieri, G. Accorsi, N. Armaroli, Chem. Commun. (2008) 2185–2193.
[51] M.D. Allendorf, C.A. Bauer, R.K. Bhakta, R.J.T. Houk, Chem. Soc. Rev. 38 (2009) 1330–1352.
[52] J. Jin, W. Wang, Y. Liu, H. Hou, Y. Fan, Chem. Commun. 47 (2011) 7461–7463.
[53] F.-J. Liu, D. Sun, H.-J. Hao, R.-B. Huang, L.-S. Zheng, Inorg. Chem. Comm. 15 (2012) 136–139.
[54] X. Huang, H. Li, Z. Tu, L. Liu, X. Wu, J. Chen, Y. Liang, Y. Zou, Y. Yi, J. Sun, W. Xu, D. Zhu, J. Am. Chem. Soc. 140 (2018) 15153–15156.
[55] J.-Y. Wang, W.-H. Li, Z. Wei, C. Zhang, Y.-H. Li, X.-Y. Dong, G. Xu, S.-Q. Zang, Chem. Commun. 56 (2020) 2091–2094.
[56] A. Seeboth, D. Lötzsch, R. Ruhmann, O. Muehling, Chem. Rev. 114 (2014) 3037–3068.
[57] R.-W. Huang, X.-Y. Dong, B.-J. Yan, X.-S. Du, D.-H. Wei, S.-Q. Zang, T.C.W. Mak, Angew. Chem. Int. Ed. 57 (2018) 8560–8566.
[58] O. Veselska, C. Dessal, S. Melizi, N. Guillou, D. Podbevšek, G. Ledoux, E. Elkaim, A. Fateeva, A. Demessence, Inorg. Chem. 58 (2019) 99–105.
[59] X. Wu, G.Y. Chen, G. Owens, D. Chu, H. Xu, Mater. Today Energy 12 (2019) 277–296.
[60] H.S. Jung, P. Verwilst, A. Sharma, J. Shin, J.L. Sessler, J.S. Kim, Chem. Soc. Rev. 47 (2018) 2280–2297.
[61] M.-Q. Li, M. Zhao, L.-Y. Bi, Y.-Q. Hu, G. Gou, J. Li, Y.-Z. Zheng, Inorg. Chem. 58 (2019) 6601–6608.
[62] D.-H. Li, J.-S. Shen, N. Chen, Y.-B. Ruan, Y.-B. Jiang, Chem. Commun. 47 (2011) 5900–5902.
[63] S. Pan, W. Liu, J. Tang, Y. Yang, H. Feng, Z. Qian, J. Zhou, J. Mater. Chem. B 6 (2018) 3927–3933.
[64] Y. Han, L. Shi, X. Luo, X. Chen, W. Yang, W. Tang, J. Wang, T. Yue, Z. Li, Carbon 149 (2019) 355–363.
[65] C. Song, B. Yang, Y. Zhu, Y. Yang, L. Wang, Biosens. Bioelectron. 87 (2017) 59–65.
[66] J.-S. Shen, D.-H. Li, M.-B. Zhang, J. Zhou, H. Zhang, Y.-B. Jiang, Langmuir 27 (2011) 481–486.
[67] T. Shu, X. Lin, Z. Zhou, D. Zhao, F. Xue, F. Zeng, J. Wang, C. Wang, L. Su, X. Zhang, Sens. Actuators B Chem 286 (2019) 198–205.
[68] Y. Zhou, W. Huang, Y. He, Sens. Actuators B Chem 270 (2018) 187–191.
[69] X. Zhao, X. Lin, J. Wang, X. Chen, New J. Chem. 43 (2019) 2790–2796.
[70] Y. Wu, X. Liu, Q. Wu, J. Yi, G. Zhang, Anal. Chem. 89 (2017) 7084–7089.
[71] Z. Li, J. Zhang, Y. Li, S. Zhao, P. Zhang, Y. Zhang, J. Bi, G. Liu, Z. Yue, Biosens. Bioelectron. 99 (2018) 251–258.
[72] Q. Zhang, Y. Hong, N. Chen, D.-D. Tao, Z. Li, Y.-B. Jiang, Chem. Commun. 51 (2015) 8017–8019.
[73] F. Shahdost-fard, M. Roushani, Biosens. Bioelectron. 87 (2017) 724–731.
[74] P. Casuso, I. Loinaz, M. Möller, P. Carrasco, J.A. Pomposo, H.J. Grande, I. Odriozola, Supramol. Chem. 21 (2009) 581–584.
[75] J.-S. Shen, D.-H. Li, Q.-G. Cai, Y.-B. Jiang, J. Mater. Chem. 19 (2009) 6219–6224.
[76] P. Casuso, P. Carrasco, I. Loinaz, G. Cabañero, H.J. Grande, I. Odriozola, Soft Matter 7 (2011) 3627–3633.
[77] S. Ilyin, T. Roumyantseva, V. Spiridonova, A. Semakov, E. Frenkin, A. Malkin, V. Kulichikhin, Soft Matter 7 (2011) 9090–9103.
[78] I. Odriozola, P. Casuso, I. Loinaz, G. Cabañero, H.J. Grande, Org. Biomol. Chem. 9 (2011) 5059–5061.
[79] P. Casuso, I. Odriozola, A. Pérez-San Vicente, I. Loinaz, G. Cabañero, H.-J. Grande, D. Dupin, Biomacromolecules 16 (2015) 3552–3561.
[80] W. Chen, H. Chen, D. Zheng, H. Zhang, L. Deng, W. Cui, Y. Zhang, H.A. Santos, H. Shen, Adv. Sci. 7 (2020) 1902099.
[81] Y. Zhou, J. Yoon, Chem. Soc. Rev. 41 (2012) 52–67.
[82] S. Chowdhury, B. Rooj, A. Dutta, U. Mandal, J Fluoresc 28 (2018) 999–1021.
[83] W. Zhai, X. Sun, T.D. James, J.S. Fossey, Chem. Asian J. 10 (2015) 1836–1848.
[84] X.-Y. Dong, H.-L. Huang, J.-Y. Wang, H.-Y. Li, S.-Q. Zang, Chem. Mater. 30 (2018) 2160–2167.
[85] J. Nan, X.P. Yan, Chem. Eur. J. 16 (2010) 423–427.
[86] A. Ruiz de Luzuriaga, A. Rekondo, R. Martin, G. Cabañero, H.J. Grande, I. Odriozola, J. Polym. Sci., Part A: Polym. Chem. 53 (2015) 1061–1066.
[87] D. Mozhdehi, S. Ayala, O.R. Cromwell, Z. Guan, J. Am. Chem. Soc. 136 (2014) 16128–16131.
[88] H. Qin, T. Zhang, H.-N. Li, H.-P. Cong, M. Antonietti, S.-H. Yu, Chem 3 (2017) 691–705.
[89] I. Odriozola, I. Loinaz, J.A. Pomposo, H.J. Grande, J. Mater. Chem. 17 (2007) 4843–4845.
[90] D.B. Amabilino, D.K. Smith, J.W. Steed, Chem. Soc. Rev. 46 (2017) 2404–2420.
[91] N. Yadav, M.K. Chauhan, V.S. Chauhan, Biomater. Sci. 8 (2020) 84–100.
[92] N. Henry, J. Clouet, J. Le Bideau, C. Le Visage, J. Guicheux, Biotechnol. Adv. 36 (2018) 281–294.
[93] E.S. Silagi, I.M. Shapiro, M.V. Risbud, Matrix Biol. 71 (2018) 368–379.